



## Petrogenesis and rare earth element mineralization of the Elk Creek carbonatite, Nebraska, USA

Philip L. Verplanck<sup>a,\*</sup>, G. Lang Farmer<sup>b</sup>, Richard M. Kettler<sup>c</sup>, Heather A. Lowers<sup>a</sup>,  
Craig A. Johnson<sup>a</sup>, Alan E. Koenig<sup>a,1</sup>, Michael J. Blessington<sup>c,2</sup>

<sup>a</sup> U.S. Geological Survey, Denver, CO 80225, USA

<sup>b</sup> Department of Geological Sciences, University of Colorado, Boulder, CO 80309, USA

<sup>c</sup> Department of Earth and Atmospheric Sciences, University of Nebraska, Lincoln, NE 68588, USA

### ARTICLE INFO

#### Keywords:

Carbonatite  
Rare earth element mineralization  
Radiogenic isotopes  
Stable isotopes  
Hydrothermal

### ABSTRACT

Although carbonatites are the primary source of the world's rare earth elements (REEs), the processes responsible for ore-grade REE enrichment in carbonatites are still poorly understood. In this study, we present a petrologic, geochemical, and isotopic evaluation of the Elk Creek carbonatite in southeast Nebraska to constrain the origin of REE mineralization. The Elk Creek carbonatite is a multilithologic carbonatite comprised of an early apatite-dolomite carbonatite, a middle/heavy REE-enriched magnetite-dolomite carbonatite, and a late-stage light REE-enriched, barite-dolomite carbonatite, as well as a suite of breccias. Neodymium, strontium, and carbon isotopic data from the early apatite-dolomite carbonatite,  $\epsilon_{Nd}(T) = 2.3$  to  $3.4$ ,  $^{87}Sr/^{86}Sr_{(i)} = 0.702704$  to  $0.702857$ , and  $\delta^{13}C = -3.3$  to  $-3.4$ , indicate that the parental magma and REEs were derived from the mantle, and textural and chemical data suggest that hydrothermal processes played an important role in reaching ore-grade enrichment. Higher initial  $^{87}Sr/^{86}Sr$  values ( $\sim 0.7041$ ) of REE-mineralized lithologies are evidence that these fluids were derived, in part, from meteoric water that interacted with the country rock. Modeling of the C-O isotopic data reveals that some of the isotopic variation results from closed-system Rayleigh fractionation of an evolving carbonatitic magma between 300 and 500 °C, but an excursion to heavier  $\delta^{18}O$  is likely the result of interaction with H<sub>2</sub>O-CO<sub>2</sub>-fluids at temperatures from 400 to 100 °C. Hydrothermal dolomite has higher  $^{87}Sr/^{86}Sr$  values than early-formed magmatic dolomite, consistent with metasomatism by fluids derived, in part, from a more radiogenic source such as the Precambrian-age wall rock. Rare earth element mineralization occurs primarily in fine-grained, cavity filling minerals including monazite, bastnäsite, parisite, and synchysite along with barite, dolomite, quartz, and iron oxides. We interpret the LREE enrichment at Elk Creek to be the product of hydrothermal fluids derived from the evolving carbonatite magma and fluids from the wall rock. The REEs likely became enriched in late-stage fluids from the evolving magma as well as being remobilized by the dissolution of earlier formed minerals. Middle/heavy REE-enrichment in the magnetite-dolomite carbonatite is hosted in hydrothermal dolomite and is attributed to variations in the composition of hydrothermal fluids.

### 1. Introduction

With the increasing reliance on high technology and green energy products, demand for critical metals has become an important driver in economic geology. Understanding how various elements reach ore-grade enrichment and what minerals host the elements of interest are two keys to successful deposit evaluation. Compared to most base and

precious metals, many critical elements tend to be enriched in relatively uncommon rocks and minerals. Carbonatites are one example of such, given that carbonatite-related deposits are the primary source of the world's rare earth elements (REEs) and niobium as well as important sources of phosphate, iron, and fluorine (Chakhmouradian and Wall, 2012; Jones et al., 2013; Verplanck et al., 2016). Currently the global supply of these critical elements (REEs and Nb) is dependent on only a

\* Corresponding author at: U.S. Geological Survey, MS 973 Denver Federal Center, Denver, CO 80225, United States.

E-mail address: [plv@usgs.gov](mailto:plv@usgs.gov) (P.L. Verplanck).

<sup>1</sup> Present address: Koenig Scientific, Rocklin, CA, 95765, USA.

<sup>2</sup> Present address: Resolution Copper, Superior, AZ 85173, USA.

few mines, and as a result there is increasing interest in determining if other carbonatites have the potential to help meet increased future demand for these elements.

Although carbonatites have been the primary source of REEs, especially light REEs (LREEs), since the 1960's, the processes responsible for ore-grade REE enrichment in carbonatites are still poorly understood (Verplanck et al., 2016; Feng et al., 2020; Wang et al., 2020). Rare earth element mineralization can be magmatic as is the case with some ore at the Mountain Pass deposit in southeast California (Mariano, 1989a), but there is increasing evidence that hydrothermal processes play an important role in many deposits (Xie et al., 2015; Trofanenko et al., 2016; Broom-Fendley et al., 2017b; Song et al., 2018; Smith et al., 2000; Ying et al., 2020; Anenburg et al., 2021; Walter et al., 2021). However, the specifics of ore-forming process during the magmatic–hydrothermal transition in carbonatites are still unclear, in part because complex textures, multiple metasomatic events, and multiple brecciation events make unravelling the paragenesis challenging.

Carbonatites are defined by the International Union of Geological Sciences (IUGS) as igneous rocks composed of greater than 50 vol% primary carbonate minerals, primarily calcite and/or dolomite, and containing less than 20 wt% SiO<sub>2</sub> (Le Maître, 2002). Physical properties of carbonate melts differ from the commonly occurring silicate magmas; these differences include a relatively low viscosity, low magmatic temperatures, and ability to incorporate relatively high amounts of volatile components compared to silicate magmas. Experimental work by Kepler (2003) showed that a Ca-Na-Mg carbonate melt at 900 °C and 1 Kbar could contain up to 10% water, approximately two to three times that of a silicate melt under similar conditions. Studies of fluid and melt inclusions in carbonatites document not only the presence of H<sub>2</sub>O and CO<sub>2</sub> but also Cl, F, P, and S, and these components can partition into a fluid phase (Bühn, 2008; Panina and Motorina, 2008; Xie et al., 2009, 2015; Prokopyev, et al., 2016). Recent experimental studies have shown that hydrothermal fluids can not only redistribute REEs but also fractionate light and heavy REEs (Williams-Jones et al., 2012; Gysi and Williams-Jones, 2013; Migdisov et al., 2016; Louvel et al., 2022). Components in fluids associated with carbonatites that may be important controls on the fate and transport of REEs include Cl<sup>-</sup>, F<sup>-</sup>, SO<sub>4</sub><sup>2-</sup>, CO<sub>3</sub><sup>2-</sup>, PO<sub>4</sub><sup>3-</sup> and OH<sup>-</sup> (Jago and Gittins, 1991; Bühn and Rankin, 1999; Williams-Jones et al., 2012; Broom-Fendley et al., 2016a, 2016b; Migdisov et al., 2016; Louvel et al., 2022). Notwithstanding these experimental efforts, there is no consensus regarding the origin of REE-mineralizing fluids or the components of REE mineralization.

Detailed petrologic, geochemical, and isotopic evaluations of mineralized carbonatites can help put laboratory-based investigations into a mineral exploration framework (Andersen et al., 2017; Ying et al., 2020). Our study focuses on the geology and geochemistry of the Elk Creek carbonatite in southeast Nebraska, which hosts the United States' largest Nb resource (Karl et al., 2021) and contains zones with high REEs concentrations, as well as being a potential resource for scandium and titanium (Brown et al., 2019). Furthermore, zones of light and middle/heavy REE-enrichment have been identified. The purpose of this investigation is to gain insight into the processes controlling REE ore-grade enrichment and the fractionation of light and heavy REEs. This study utilized archived drill core samples and presents petrographic and mineral chemistry results to determine the relative timing of various carbonatite lithologies and determine if the minerals are primary magmatic or hydrothermal in origin. Whole-rock geochemistry results are used to evaluate magmatic trends, identify zones of REE enrichment and fractionation, and guide isotopic work. Isotopic results help to constrain the origin of the REEs and fluids.

## 2. Geologic setting

The Elk Creek carbonatite is an elliptical body approximately 6–8 km in diameter located in southeast Nebraska. It is part of a Cambrian-Ordovician alkaline complex that is buried by approximately 200 m of

Pennsylvanian marine sedimentary rocks and Quaternary glacial till (Carlson and Treves, 2005). The alkaline complex occurs on the eastern margin of the Midcontinent rift system where the rift has been offset by one of a series of southeasterly-trending structures. This particular structure extends into northeastern Missouri where it has been mapped as the Missouri gravity low (Van Schmus et al. 1996) or the south central magnetic lineament (Atekwana, 1996). The Elk Creek carbonatite is located near the boundary between the Proterozoic Yavapai and Mazatzal provinces, which are two blocks of juvenile crust (Whitmeyer and Karlstrom, 2007). The carbonatite, and associated alkaline units, intruded Proterozoic granites and gneisses of the Nemaha uplift. Because of the sedimentary cover, there is no surface expression of the Elk Creek alkaline rocks. In some drill cores the unconformity between the carbonatite and overlying sedimentary units is marked by paleosols that developed within carbonatite, suggesting that at some time the carbonatite was exposed to subareal weathering (Nicklen and Joekel, 2001). Most drill holes ended within the carbonatite, and geophysical modelling suggests that the intrusion is open at depth (Drenth, 2014).

### 2.1. Previous work

The carbonatite was discovered in 1970 through a regional geophysical survey which defined a circular, positive gravity anomaly in southeast Nebraska. The following year, the Conservation and Survey Division of the University of Nebraska-Lincoln drilled this location and encountered iron-rich carbonate rocks that were identified as carbonatite (Burfeind et al., 1971). The Molybdenum Corporation of America (MolyCorp) leased property in the area and drilled 106 holes into the carbonatite between 1973 and 1986. In 2010, Quantum Rare Earth Developments Corporation, now called NioCorp Development Ltd., acquired access to the property and drilled additional holes (Brown et al., 2019).

MolyCorp evaluated the deposit for REEs and Nb and initiated a lithologic naming convention based on mineralogy and textures. Carbonatite units included apatite beforite, magnetite beforite, barite beforite, and beforite breccias (beforite being the term used for dolomite-rich carbonatite). Mafic rocks were identified as xenoliths in beforite units, as clasts in breccias, and as dikes that crosscut carbonatite lithologies. MolyCorp noted extensive zones of fenitization, ferruginous alteration, and brecciation (Mariano, 1976).

Brookins et al. (1975) undertook a Sr isotopic study and concluded that fifteen samples were consistent with a carbonatite origin (0.7030–0.7055) and three samples had distinctly higher ratios (0.7064–0.7085), suggesting input from sedimentary carbonate and/or contamination by other non-carbonatite material. Utilizing the archived drill core from MolyCorp, along with a high-resolution airborne gravity gradient and magnetic survey, compiled MolyCorp drill core lithology data, and new measured physical properties of drill core samples, Drenth (2014) described the geophysical expression of the Elk Creek carbonatite. The new geophysical survey, coupled with the drill core descriptions, enabled Drenth (2014) to delineate the horizontal extent of the carbonatite which is approximately 4.5 by 7 km (Fig. 1).

Limited age dating of the Elk Creek complex has been undertaken. Two potassium-argon determinations for biotite in an altered basalt yielded dates of 464 ± 5 and 484 ± 5 Ma (personal communications M. Ghazi, Georgia State University, reported by Carlson and Treves, 2005). A potassium-argon determination of another biotite from a silicate rock yielded an age of 544 ± 7 Ma. (personal communications Z.E. Peterman, United States Geological Survey, 1985, reported by Carlson and Treves, 2005).

## 3. Methods

This study is based on samples from MolyCorp Inc. drill cores archived at the University of Nebraska-Lincoln. Between 1973 and 1986 MolyCorp drilled 106 holes into the carbonatite, and approximately

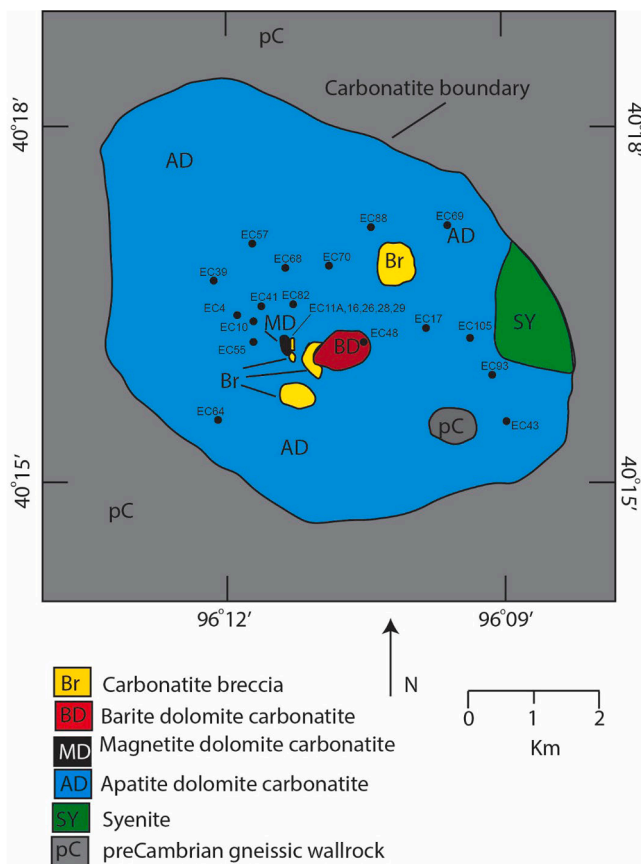


**Fig. 1.** Simplified geologic map of the Elk Creek carbonatite at an elevation of 120 m, approximately 230 m below ground surface, using MolyCorp drill core lithologic data, with younger mafic dikes removed (adapted from Drenth, 2014). Sampled drill core collar location are displayed.

24,400 m of cores and rotary samples were recovered. The primary focus of the study was on the carbonatite lithologies, but six alkaline silicate rock samples were analyzed for major and trace element chemistry, four of which were analyzed for their Nd and Sr isotopic compositions. Mineralogy and petrology were studied in transmitted and reflected light using an optical microscope followed by the utilization of scanning electron microscopy (SEM). Eight-seven geochemical samples were collected from sections of drill core. In addition, the drill core archive included ten-foot composite chip samples, and a subset of these, forty-six samples, were analyzed.

### 3.1. Whole-rock major- and trace-element analysis

Rocks were pulverized in a ceramic container, and major and trace element data were obtained from SGS Mineral Services, Canada and AGAT Laboratories, Canada. Major element analyses were performed by wavelength-dispersive X-Ray fluorescence (WDXRF) with analytical uncertainties of less than 5%. Minor and trace element determinations were performed using inductively coupled plasma-optical emission spectrometry (ICP-OES) and inductively coupled plasma mass spectrometry (ICP-MS) with analytical uncertainties of less than 15% of the reported values. In addition, one U.S. Geological Survey (USGS) standard reference material was submitted per every ten samples to verify analytical uncertainty. Data are presented in [Supplementary data Table 1](#).

### 3.2. Element analysis of minerals

Major element analyses of dolomite grains were determined by

electron microprobe analysis (EPMA) at the USGS in Denver, Colorado ([Supplementary data Table 2](#)). Quantitative elemental analysis of coated polished grain mounts of dolomite using EPMA were acquired with a fully automated JEOL 8530F Plus electron microprobe equipped with five wavelength X-ray spectrometers. Operating conditions were 12 kV, 20 nA (cup), 2  $\mu$ m beam diameter, and 40 s on the peak and 20 s on the background. Well-characterized silicate and oxide mineral standards were used for calibration. CO<sub>2</sub> was added by difference from a total of 100% to the sum of analyzed elements. The data were normalized to 6 oxygens to calculate stoichiometric compositions. ZAF matrix corrections were used. The analytical errors for EPMA were approximately  $\pm 5$  percent of the reported values for major and minor elements (Ca, Mg, Fe, Mn) based on replicate analyses of laboratory standards. Values for major and minor elements are reported in weight percent. Points that contained contributions from surrounding phases, such as silicates or iron oxides, were removed from the dataset based on high Si and Fe values.

Rare earth element concentrations of the dolomite and apatite grains ([Supplementary data Table 3](#)) were determined using Laser Ablation Inductively Coupled Plasma Mass Spectrometry (LA-ICP-MS) hosted at USGS-Denver following the procedure of Koenig et al. (2009). Apatite and dolomite mineral grains were ablated directly from polished thin sections and analyses were conducted using a Photon Machines Analyte G2 LA system (193 nm, 4 ns excimer) attached to a Perkin Elmer DRC-e ICP-MS. Prior to ablation, petrographic and scanning electron microscope analyses were undertaken to identify homogeneous domains. The ablation spot size varied from 30  $\mu$ m for apatite grains to 150  $\mu$ m for dolomite grains with an 8 Hz repetition rate and energy density of 4 J/cm<sup>2</sup>. Single spot analyses were ablated using six pulses per second. Ablated materials were transported via a He carrier gas to a modified glass mixing bulb where He and the ablated materials mixed coaxially with Ar prior to the ICP torch. Signals were screened visually for heterogeneities such as micro-inclusions or zoning. The detection limit for LA-ICP-MS is below 0.01 ppm for most elements, and run precision is better than 10% of the reported values based on reproducibility of standards.

### 3.3. Multi-isotope analysis

Sample splits for whole-rock Nd and Sr isotopic determinations were obtained from the prepared samples for major and trace element chemistry. Strontium and Nd isotope analyses were undertaken at the University of Colorado, Boulder. Whole-rock samples were dissolved in open containers in HCl, HF and HClO<sub>4</sub>. Dolomite separates were collected using a micromill on thin section billets such that for samples with multiple generations of dolomite, the sample may not represent 100% of a mineral phase. Prior to micro milling, mineral locations were identified by petrographic and scanning electron microscope study of thin sections made from the respective billets. The Sr and Nd isotopic compositions of whole-rock samples and mineral separates ([Supplementary data Tables 4 and 5](#)) were obtained using a Finnigan-MAT 261, six collector, solid source, mass spectrometer (Farmer et al., 1991). The mean value for the SRM987 standard during this period was  $0.71027 \pm 2$  ( $2\sigma$  standard error), and the mean value for the LaJolla Nd standard during this period was  $0.511836 \pm 9$  ( $2\sigma$  standard error). The resulting  $\epsilon_{Nd}$  values and initial  $^{87}Sr/^{86}Sr$  values were calculated at 571 Ma.

Carbon and oxygen isotope ratios were measured at the stable isotope laboratory of the Geology, Geophysics, and Geochemistry Science Center, USGS, Denver, Colorado using a Micromass Optima mass spectrometer system that utilizes phosphoric acid digestion in septum-capped vials at a temperature of 90 °C (Verplanck et al., 2022). The system was calibrated by analyzing aliquots of the NBS 18 and NBS 19 calcite standards along with the unknowns (accepted values taken from Brand et al., 2014). Results are expressed in  $\delta$ -notation relative to Vienna Pee Dee Belemnite (VPDB) for carbon and Vienna Standard Mean Ocean Water (VSMOW) for oxygen. Their estimated error is  $\pm 0.1\%$  for both.

The acid fractionation factor for oxygen isotopes differs slightly between calcite and dolomite, however no attempt was made to correct the dolomite  $\delta^{18}\text{O}$  values for this difference because the correction is both imperfectly known and insignificant for the purposes of this study (Kim et al., 2015).

#### 4. Results

##### 4.1. Lithologic and petrographic characterization

Dolomite is the primary carbonate mineral within the complex and occurs in every carbonatite lithology such that all carbonatite units have been subdivided based on the second most abundant mineral (apatite, magnetite, or barite). The three main carbonatite lithologies are the

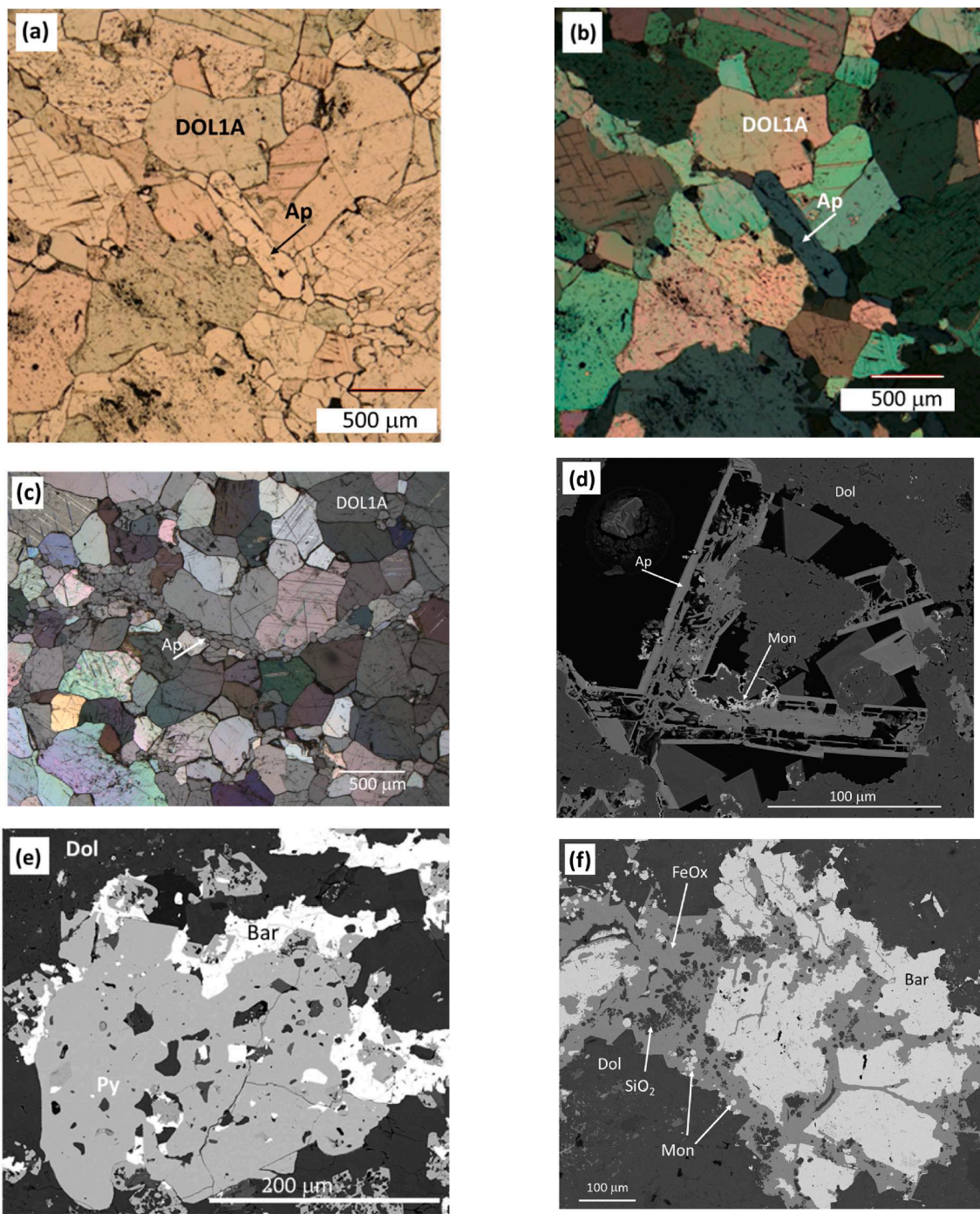


**Fig. 2.** Photomicrographs and back-scatter electron images (BSE) displaying mineral textures in the apatite-dolomite carbonatite unit. (a) Plane-polarized light photomicrograph of fresh apatite-dolomite carbonatite with euhedral to subhedral apatite grains and dolomite; (b) Cross-polarized light photomicrograph of the same section; (c) Cross-polarized light photomicrograph of fresh apatite-dolomite carbonatite with bands of euhedral to subhedral apatite; (d) BSE image of apatite-dolomite carbonatite with corroded apatite and cavity, bright spots on corroded apatite are monazite; (e) BSE image of corroded and embayed pyrite grain; and (f) BSE image of cavity filled with barite, iron oxide, quartz, and monazite. Mineral abbreviations: Ap = apatite, Dol = dolomite, FeOx = iron oxide phase, Mon = monazite, Py = pyrite, SiO<sub>2</sub> = silica phase.

apatite-dolomite (AD) carbonatite, the magnetite-dolomite (MD) carbonatite, and the barite-dolomite (BD) carbonatite. Similar to most mineralized carbonatites, carbonatite breccias are present and hydrothermal alteration overprints many primary features. The AD carbonatite is the dominant lithology, forming approximately 70 percent by volume of this large carbonatite complex (Fig. 1). The other two carbonatite lithologies, the MD and BD carbonatites, are substantially lower in volume, approximately 2 and 6% respectively, with the remaining carbonatite comprising brecciated units or undifferentiated carbonatite units (Drenth, 2014). Textural relationships and chemical trends observed in this study suggest that the AD carbonatite is the oldest carbonatite unit followed by the MD dolomite carbonatite and the BD carbonatite.

The AD carbonatite consists of dolomite and apatite with accessory biotite, phlogopite, barite, sulfides (dominantly pyrite), pyrochlore, magnetite, fluorite, quartz, and REE-rich phases. The REE minerals are monazite and REE-fluorocarbonate minerals, primarily parisite and synchysite with subordinate bastnäsite. The abundance of apatite varies from trace to approximately fifteen percent. Texturally, the AD carbonatite is quite variable, varying from coarse-grained and composed almost entirely of dolomite to fine-grained, with or without flow banding. Vugs are present in some AD carbonatite samples. The least altered AD carbonatites are located the furthest from the MD and BD carbonatites and consist of medium to coarse-grained dolomite with apatite (Fig. 2a-c). The dolomite is well-crystallized, contains inclusions, and is intergrown with coarse apatite. Texturally, the coarse-grained dolomite has well-developed cleavage and triple-junction grain boundaries. This is referred to as dolomite 1A (DOL1A). The apatite is subhedral to euhedral, zoned, and is either disseminated or occurs in bands and clusters (Fig. 2a, c). Near the center of the complex, the AD carbonatite contains a second dolomite (DOL2A) that rims and bisects DOL1A (Fig. 3a, b) or displays a gradational transition to DOL1A. DOL2A is fine-grained, cryptocrystalline and can be the dominant form of dolomite in a sample. Subhedral to euhedral, zoned apatite occur with DOL2A, but corroded, skeletal apatite grains have been observed (Fig. 2d). Pyrochlore, the primary Nb host mineral, occurs sporadically in the AD unit. This mineral generally forms euhedral to subhedral zoned crystals up to ~2 mm that are often broken (Fig. 4a, b), but also occurs as fine-grained euhedral to subhedral crystals in the dolomite (Fig. 4c, d). Pyrite is the main sulfide identified and occurs as either euhedral crystals or with irregular and embayed masses (Fig. 2e). The REE phases primarily occur in vugs either as fluorocarbonates or monazite (Fig. 5a, b). Monazite is also observed along apatite grain boundaries. Quartz and barite may occur as fine-grained masses and are commonly associated with the REE mineral phases (Fig. 2f). Iron oxide has been observed in these cavities (Fig. 2f). A few fluorite veinlets have been observed. Zones within the AD carbonatite contain barite as a dominant mineral phase, greater than apatite, and these zones are referred to as the barite-dolomite carbonatite, described below.

The magnetite-dolomite carbonatite occupies a small, well-delineated zone near the center of the carbonatite (Fig. 1). This unit has been extensively drilled because it is the primary host of Nb mineralization and is the focus of recent Sc and Ti assessment activities. Along with magnetite and dolomite this lithology contains variable amounts of pyrochlore, ilmenite, rutile, hematite, and sulfides. The MD carbonatite is fine grained and dark (Fig. 6a). Fresh samples are strongly magnetic and contain fine-grained euhedral magnetite (Fig. 6b). Much of this unit is brecciated, altered, and nonmagnetic. Embayed and corroded magnetite is present (Fig. 6c) and may be partially to completely replaced by ilmenite and hematite. Dolomite in this unit occurs as coarse-grained porphyritic masses or fine-grained matrix material. The porphyritic masses, texturally similar to DOL1A as described above and will be referred to as DOL1B, are surrounded by fine-grained dolomite, similar to DOL2A and referred to as DOL2B in this unit. These DOL1B fragments in the MD carbonatite are either angular pieces or rounded, elongate masses (Fig. 7a-c).

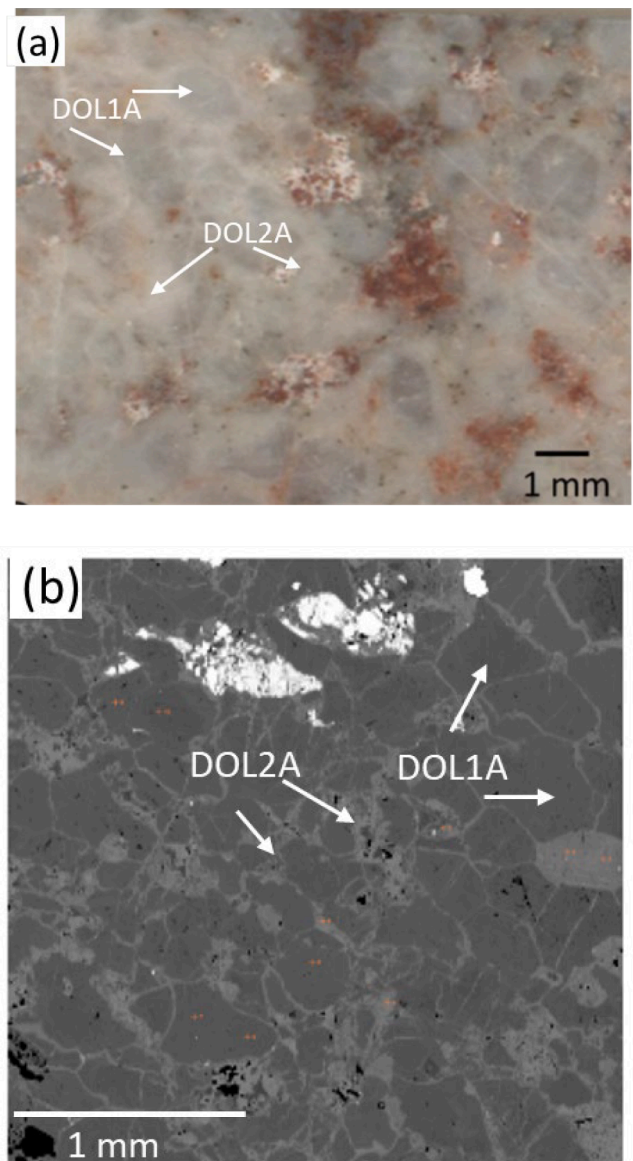
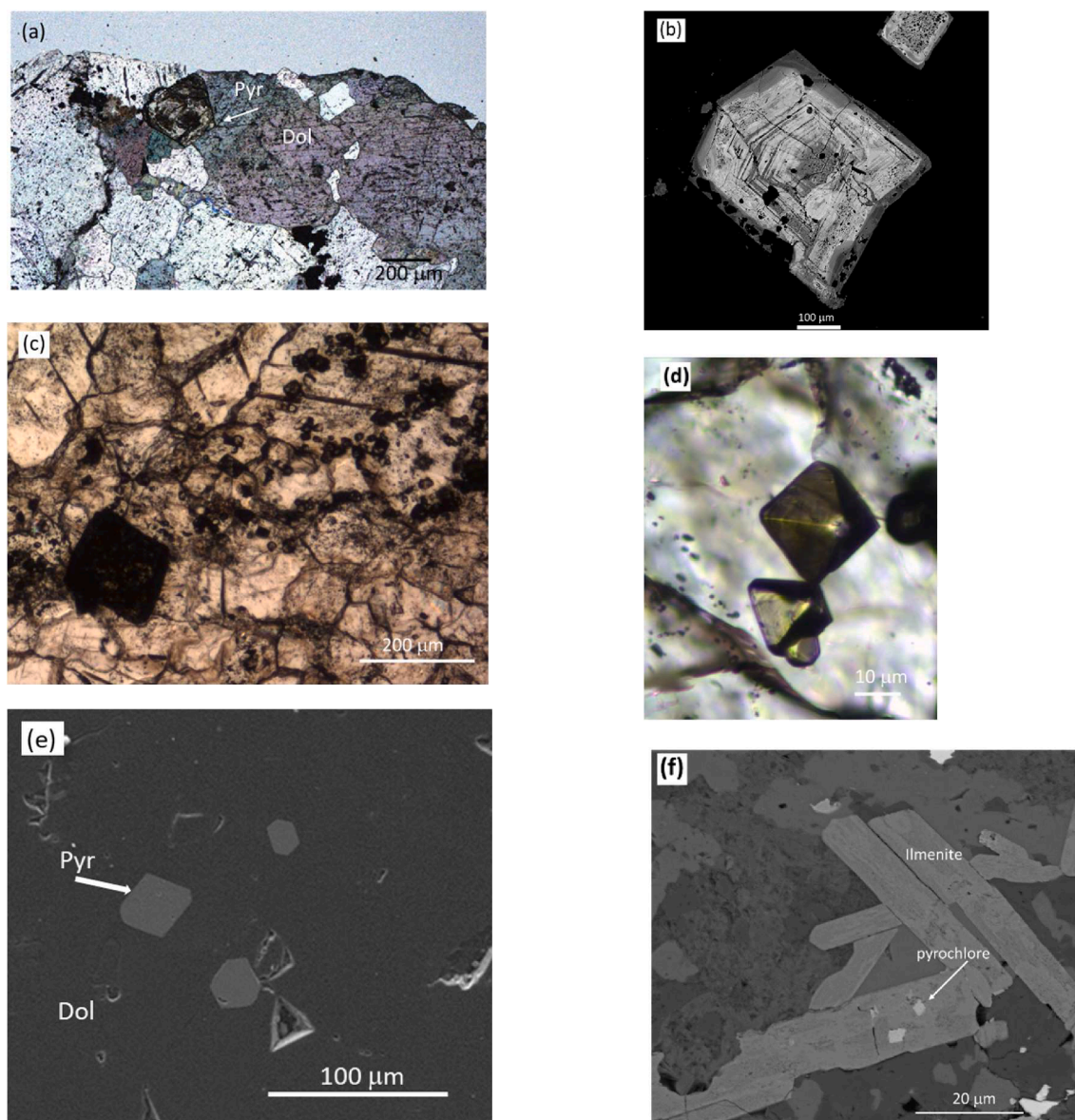


Fig. 3. Photograph and BSE image of dolomite 1 and 2 (DOL1A and DOL2A) in apatite-dolomite carbonatite. (a) Polished thin-section billet with early gray DOL1A surrounded by whiter DOL2A (EC48-971.8); and (b) BSE image of DOL2A (lighter) along boundaries of DOL1A.

Within the MD carbonatite, pyrochlore occurs as fine-grained euhedral to anhedral grains that are substantially smaller, generally <30  $\mu\text{m}$ , than the coarse-grained and zoned pyrochlore observed in the AD carbonatite. Blessington (2014) noted zones of abundant, anhedral, <10  $\mu\text{m}$ -diameter pyrochlore within the MD carbonatite that typically occurs as inclusions in ilmenite and magnetite (Fig. 4f). Veinlets of barite and dolomite are common, as discussed below. Rare earth element mineral phases, monazite and fluorocarbonates, primarily occur as vugs or cavities fillings. These cavities may also contain barite, quartz, iron oxide, potassium feldspar, and rarely, thorium minerals.

The barite-dolomite carbonatite contains the highest abundance of REE phases. Rare earth phases include parisite, synchysite, bastnäsite, and monazite. The BD carbonatite consists mainly of dolomite, barite, and quartz with minor or variable apatite, fluorite, phlogopite, pyroxene, feldspar, chlorite, and sulfides (primarily pyrite). This unit primarily occurs as veins and dikes, a few millimeters to meters in width, but thicker zones (tens of meters thick) with diffuse contacts have been identified. BD carbonatite veins crosscut both the AD and MD



**Fig. 4.** Photomicrographs and BSE images displaying pyrochlore mineral occurrences in the Elk Creek carbonatite. (a) Cross-polarize light photomicrograph of coarse-grained, zoned pyrochlore in AD carbonatite; (b) BSE image coarse-grained, zoned pyrochlore; (c) Photomicrograph of medium-size pyrochlore within dolomite (image from Blessington, 2014); (d) Photomicrograph in high magnification of euhedral, medium-size pyrochlore within dolomite (image from Blessington, 2014); (e) BSE image of euhedral, medium-size pyrochlore within dolomite; and (f) BSE image of  $<10\ \mu\text{m}$  pyrochlore in ilmenite in the MD carbonatite unit. Dol = dolomite and Pyr = pyrochlore.

carbonatites (Fig. 8a-c). Spatially, the BD carbonatite primarily occurs in zones towards the center of the carbonatite, but no discrete area of ore-grade REEs has been identified. The BD carbonatite makes up the matrix material in some of the breccias. Veins typically consist of barite, dolomite, and REE mineral phases, but an array of minerals may be associated with the veins or in the alteration halo that surround some veins. These minerals include apatite, monazite, xenotime, fluorite, bastnäsite, parisite, synchysite, pyrite, quartz, potassium feldspar, and iron oxide. Rare earth mineralization is discussed below.

Carbonatite breccias have been identified in drill core, primarily in the central part of the carbonatite associated with the MD carbonatite. Clasts within the breccia can be AD carbonatite, MD carbonatite, or mafic lithologies, with MD carbonatite clasts being the most common. BD carbonatite clasts have not been identified, but some carbonatite clasts do contain BD carbonatite veinlets. Matrix material is typically fine-grained dolomite, commonly with fine-grained barite. Much of the MD carbonatite is brecciated, with MD carbonatite occurring as clasts

and/or as the matrix.

Lithologic information from drill core is primarily focused on the carbonatite lithologies of the Elk Creek alkaline complex because mineralization in the carbonatite was the target of this study. Intercepts of syenites and mafic dikes were encountered in the drilling. The altered syenite occurs as fenitized blocks within the carbonatite. The syenite sampled in this study contains remnant orthoclase, phlogopite, and biotite, and have been substantially metasomatized with secondary dolomite.

Alteration is observed within the uppermost few meters (0 to  $\sim 15\ \text{m}$  below the Pennsylvanian contact) of the carbonatite and in zones well below the top of the carbonatite. Nicklen and Joeckel (2001) and Joeckel and Nicklen (2007) describe the upper alteration zone as containing illitic clays, leached saprolite, and saprolite consisting of hematite, goethite, and relic minerals from the underlying carbonatite. They interpreted this zone as a paleoweathering surface on the carbonatite. Within the carbonatite, zones of ferruginous alteration occur and

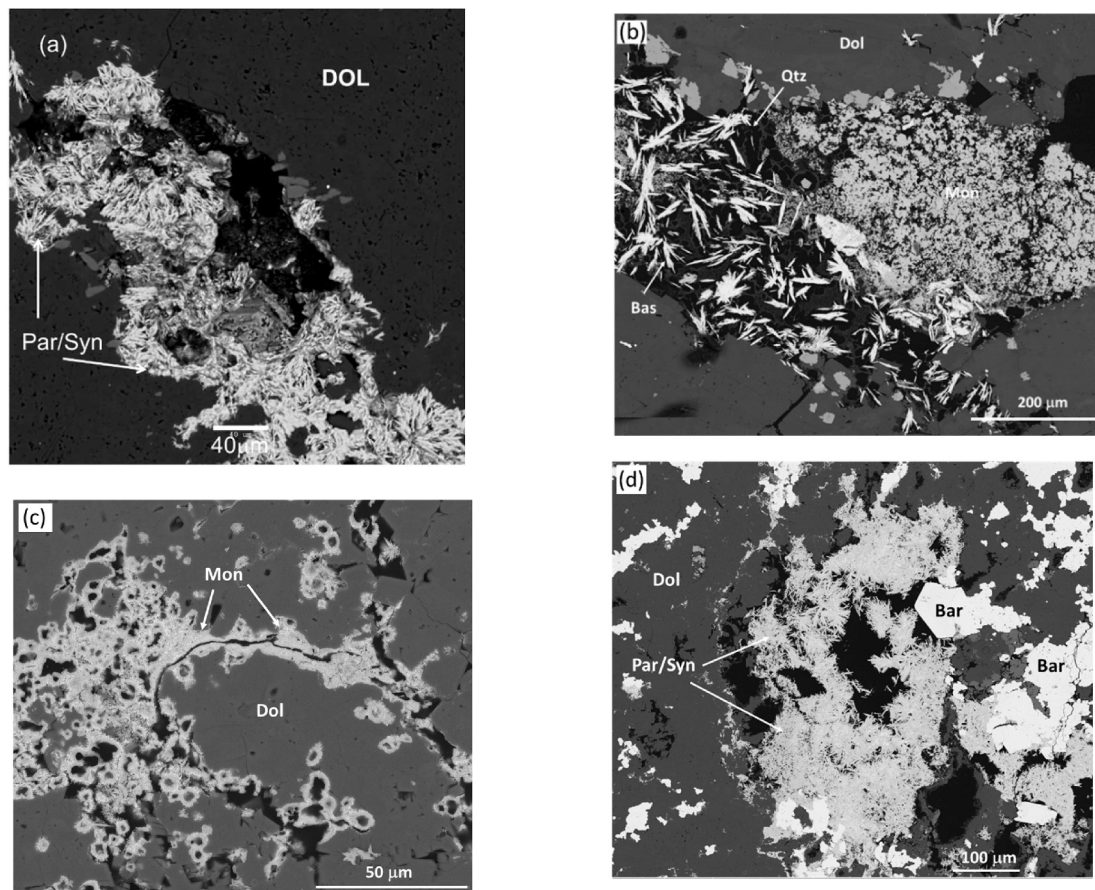


**Fig. 5.** BSE images of REE occurrences in apatite-dolomite and barite-dolomite carbonatite units. (a) Vug in apatite-dolomite carbonatite with syntaxial intergrowths of parisite and synchysite; (b) Cavity in AD carbonatite with monazite and bastnäsite infilled with quartz; (c) Fine-grained monazite along fractures and in voids, BD carbonatite; and (d) Cavity in BD carbonatite with syntaxial intergrowths of parisite and synchysite, barite, and iron oxide mineral. Mineral abbreviations: Ap = apatite, Bar = barite, Bas = bastnäsite, Dol = dolomite, FeOx = iron oxide phase, Mon = monazite, Par = parisite, Qtz = quartz, and Syn = synchysite.

range from fracture surfaces to zones with complete overprinting for tens of meters of core (Fig. 9). Intensely altered zones vary in color from yellow to dark red. Alteration minerals include hematite, limonite and quartz. In pervasively altered zones, the primary minerals and textures are difficult to recognize. In addition, some BD carbonatite veinlets are surrounded by narrow halos of bleached rock (Fig. 8c). Detailed petrographic and scanning electron microscope work documents significant hydrothermal alteration in zones of the carbonatite and which is discussed below.

#### 4.2. Rare earth element mineralization

Rare earth minerals occur in all carbonatite lithologies, with the highest abundance in the BD carbonatite. Monazite and fluorocarbonate minerals, primarily parisite and synchysite, have similar characteristics to Mariano's (1989a and 1989b) description of hydrothermal REE minerals. In the least altered AD carbonatite, the two most abundant minerals are dolomite and apatite with apatite being the primary REE host mineral. Within this unit, fine-grained needles of monazite occasionally occur along apatite grain boundaries or in vugs, similar to an example described by Chakhmouradian et al. (2017) at Miaoya, China. In the more altered AD carbonatite towards the center of the complex, monazite and REE fluorocarbonates are observed in cavities and have a range of mineral associations. Cavities within this unit may be partially filled with fibrous to acicular, syntaxial intergrown parisite and synchysite along with barite, with bladed bastnäsite, monazite and barite, with monazite and barite, and with monazite, barite, quartz, and iron oxide (Figs. 2f, 5a and b). Monazite is observed along cracks and grain

boundaries (Fig. 5c). Monazite primarily occurs as fine-grained, radiating clusters or fine needles. Parisite and synchysite are more common than bastnäsite, occurring as clusters of fine needles, sometimes in a radiating morphology (Fig. 5d).

Rare earth element mineral occurrences in the MD carbonatite are broadly similar to occurrences described above for the adjacent AD carbonatite. Barite-rich vugs and cavities with REE minerals and iron oxide are more common, and the cavities are larger in the MD carbonatite than the AD carbonatite. In cavities in the MD carbonatite, a variety of minerals are observed with the REE minerals including barite, dolomite, quartz, iron oxide, potassium feldspar, and a thorium phase. Monazite may occur along dolomite and magnetite grain boundaries (Fig. 6d).

The most common mineral associated with REE mineralization in the Elk Creek carbonatite is barite, either within or adjacent to barite veins or in vugs and cavities. Occurrences include cavities with barite, parisite/synchysite intergrowths and iron oxide and cavities with dolomite, monazite, and iron oxide. Other more complex assemblages occur within and adjacent to veinlets and include a suite of parisite/synchysite intergrowths with iron oxide and adjacent fluorite. Another example is a barite veinlet with synchysite and adjacent apatite with xenotime.

#### 4.3. Major element chemistry

On the carbonatite ternary diagram, apatite-dolomite carbonatite samples from the Elk Creek complex primarily plot in the Mg carbonatite field (Fig. 10). Petrographic analysis of the AD carbonatite shows that many AD carbonatite samples display metasomatic features, but a subset

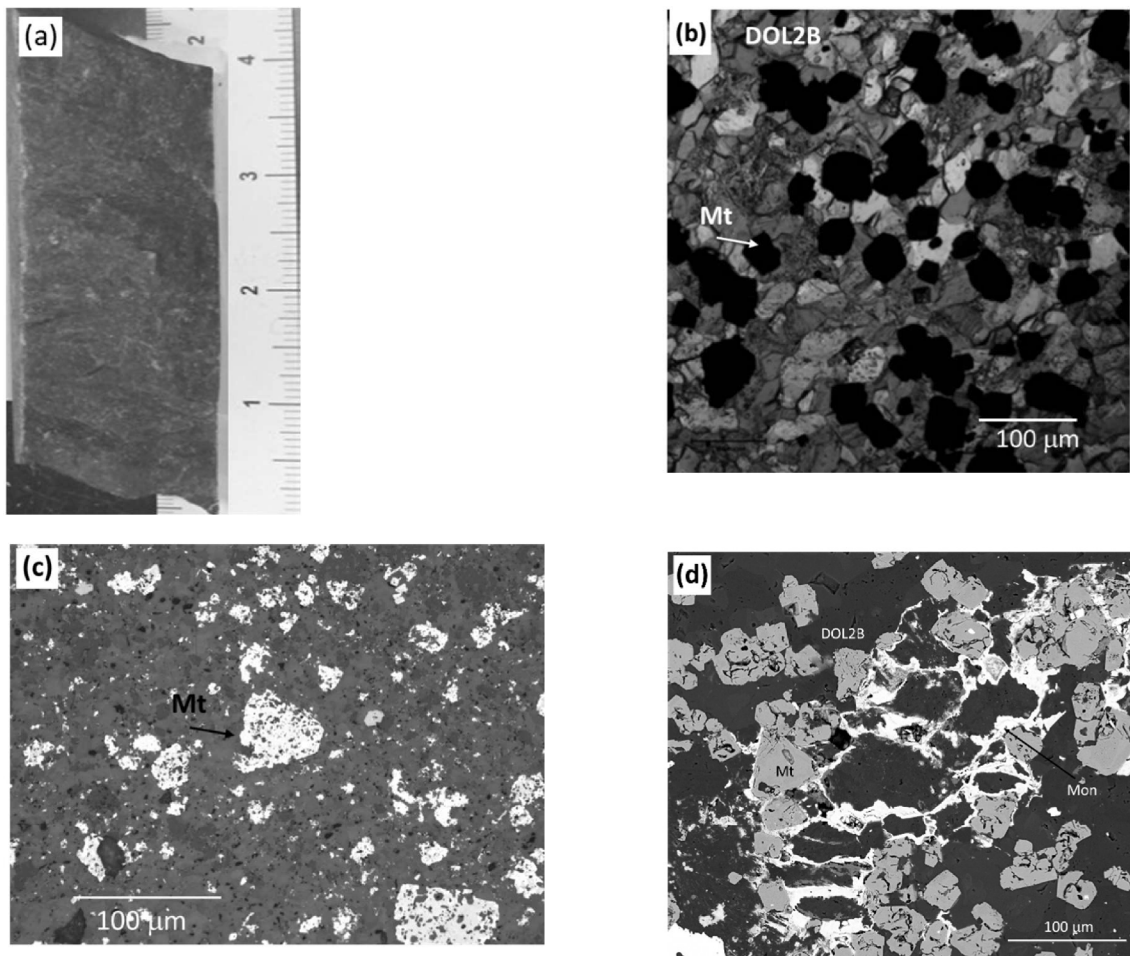


**Fig. 6.** Photograph, photomicrograph, and BSE image of the magnetite-dolomite carbonatite. (a) Drill core image of magnetite-dolomite carbonatite; (b) Cross-polarized light photomicrograph of fresh MD carbonatite; (c) Reflected light photomicrograph of MD carbonatite with embayed and corroded magnetite; and (d) BSE image of magnetite with monazite along grain boundaries and as void filling. Mineral abbreviations: Dol = dolomite, Mon = monazite, and Mt = magnetite.

of samples was delineated that are fresh to minimally altered. These samples plot in a narrower field on the low Fe portion of the ternary diagram (Fig. 10). The AD carbonatite samples are typical of many dolomite carbonatites with elevated MgO, and low Al<sub>2</sub>O<sub>3</sub>, Fe<sub>2</sub>O<sub>3</sub>, K<sub>2</sub>O, MnO, Na<sub>2</sub>O, and SiO<sub>2</sub> (Supplementary data Table 1). Consistent with the presence of apatite, the P<sub>2</sub>O<sub>5</sub> is also elevated, up to 7.54 wt%.

On the ternary diagram (Fig. 10), the MD carbonatite samples plot in a field between the AD carbonatite samples and the Fe endmember. Similar to the AD carbonatite, these samples are overprinted by fluids to varying degrees and many are crosscut by veinlets containing variable amounts barite, quartz, phosphate minerals, and fluorocarbonate minerals. Concentrations of Fe<sub>2</sub>O<sub>3</sub>, MgO, Al<sub>2</sub>O<sub>3</sub>, SiO<sub>2</sub>, and TiO<sub>2</sub> are higher in the MD carbonatite (Supplementary data Table 1) as compared to the fresh AD carbonatite samples.

The BD carbonatite samples plot in the Mg carbonatite field, overlapping the field of the AD carbonatite on the ternary carbonatite diagram (Fig. 10). Barium concentrations range from 11,200 to 143,000 ppm, such that in this unit, Ba can be considered a major element. The P<sub>2</sub>O<sub>5</sub> and SiO<sub>2</sub> concentrations are quite variable, from 0.14 to 22.6 wt% and 0.21 to 26.0 wt% respectively.

A few samples of alkaline silicate rocks were analyzed. Although these are referred to as syenites, the major element chemistry is clearly affected by hydrothermal alteration. Typical of fenitization, enrichment in CaO, K<sub>2</sub>O, and Na<sub>2</sub>O occurred at the expense of SiO<sub>2</sub> (9.8 to 36.3 wt%; Supplementary data Table 1).

#### 4.4. Minor element chemistry

As with most mineralized carbonatites, the Elk Creek carbonatite is enriched in large ion lithophile elements including Ba, Sr, and the REEs (Verplanck et al., 2016). A range in LREE enrichment in the AD carbonatite is observed, with the relatively fresh samples having lower REE concentrations (Fig. 11a). The La vs. wt % P<sub>2</sub>O<sub>5</sub> plot (Fig. 12a) for all AD carbonatite samples displays a linear relationship for many of the samples, including the suite of relatively fresh samples. Samples that lie above this trend contain vugs with REE-rich fluorocarbonates and monazite (Fig. 5a). Strontium concentrations in AD are variable and do not correlate with Ca (Fig. 12b). Barium concentrations in the AD carbonatite are variable, and elevated concentrations tend to be in samples containing fine-grained barite or those cut by barite-rich veinlets. Fluorine concentrations are variable, ranging from 200 to 11,200 ppm. Fluorine concentrations generally correlate with phosphate concentrations (Fig. 12c). Samples with greater than 4000 ppm F lie above this trend and contain fluorite or fluorocarbonate minerals either within veinlets, along fractures, or in vugs. Niobium concentrations in the AD carbonatite tend to be low, less than a few hundred ppm, except in samples that contain pyrochlore.

The REE patterns of the MD carbonatite contain a pronounced enrichment in the middle REEs (Fig. 11b), unlike the light REE-enriched patterns that most carbonatites display. The middle REE-enriched patterns have their maximum at either Eu, Gd, or Tb. Note that this manuscript denotes these elements as middle REEs but other workers, for example Broom-Fendley et al. (2016b, 2017a), demark heavy REEs

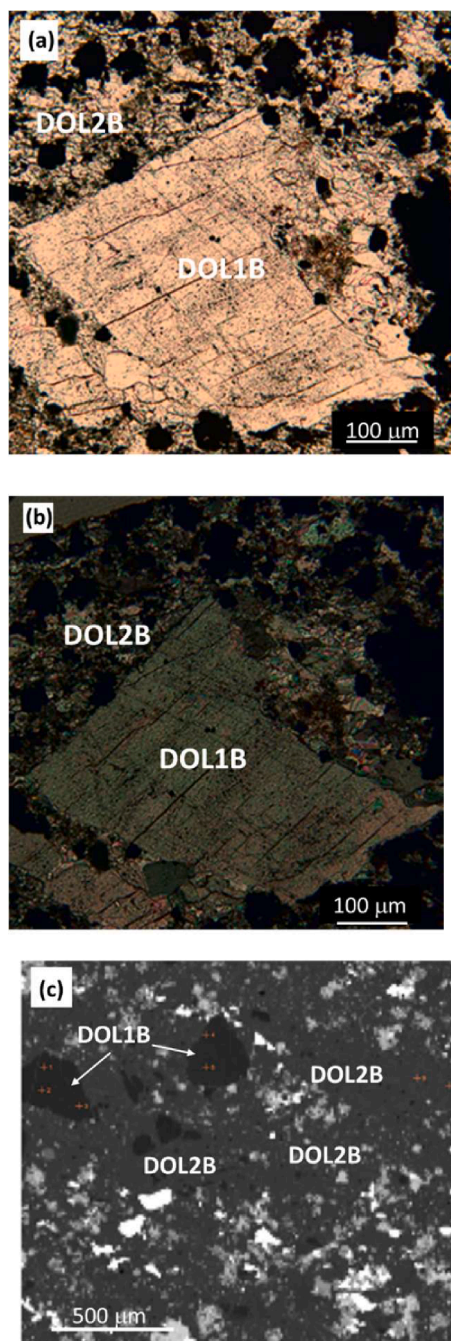


**Fig. 7.** Angular clasts of coarse-grained AD carbonatite (DOL1B) within magnetite-dolomite carbonatite (DOL2B). (a) Plane-polarized light photomicrograph; (b) Cross-polarize light photomicrograph; and (c) BSE image with DOL1B as dark clast and DOL2B as lighter gray matrix.

with mass greater than Sm. Thus, these MD carbonatite REE patterns could be classified as HREE-enriched. Some samples display enrichment in LREEs as well, and these samples contain veinlets with barite, quartz and fluorocarbonate or phosphate minerals. Barium concentrations in the MD carbonatite are variable, 2000 to 151,000 ppm, and elevated Ba concentrations occur in samples crosscut by barite veinlets. The MD carbonatite is the primary exploration target for Nb, Sc, and Ti. Compared to the other carbonatites at Elk Creek, these elements are enriched in most MD carbonatite samples (Fig. 13 a-c). Niobium variation is correlated with Ti but not Sc, suggesting that Sc, at least in part, resides in different mineral phases than Nb. Similar to the AD, fluorine concentrations are variable, 410 to 61,400 ppm, and samples with high



**Fig. 8.** Photographs of hand samples of barite-dolomite carbonatite veinlets crosscutting apatite-dolomite carbonatite and magnetite-dolomite carbonatite. (a) apatite-dolomite carbonatite with veins of barite-dolomite carbonatite. Reddish-brown color of veins primarily from iron oxide minerals, (b) magnetite-dolomite carbonatite with veins of barite-dolomite carbonatite. Reddish-brown color of veins primarily from iron oxide minerals; and (c) magnetite-dolomite carbonatite with veins of barite-dolomite carbonatite displaying extensive alteration halo around veins.

concentrations contain fluorite veinlets.

The BD carbonatite REE patterns display LREE-enrichment and a steep negative slope on the chondrite-normalized REE diagram (Fig. 11c). The La, Ce, Pr, and Nd concentrations overlap those of ore-grade concentrations at actively mined carbonatite deposits of Mountain Pass, Bayan Obo, and Maoniuping (Verplanck et al., 2016). Fluorine concentrations range from 360 to 37,100 ppm. Niobium concentrations are relatively low (29–1720 ppm, with a median value of 660 ppm) compared to other carbonatite lithologies in the Elk Creek complex. Although this unit is enriched in Ba and LREEs, thorium concentrations are not enriched, 24.3 to 361 ppm, compared to the MD carbonatite.

#### 4.5. Mineral chemistry

Electron microprobe spot analyses were conducted on dolomite 1 and 2 crystals, which are reported in Supplementary data Table 2. DOL1A in the least altered AD carbonatite has similar median concentrations of Fe and Mn (2.2% and 0.7%, respectively, n = 32) to DOL1A that is surrounded by DOL2A in the altered AD carbonatite (2.2% Fe and 0.7% Mn, n-14), and to the DOL1B clasts within the MD carbonatite



Fig. 9. Photograph of drill core photograph of zone of Elk Creek carbonatite overprinted by extensive iron oxidation, core depth of 2265 feet.

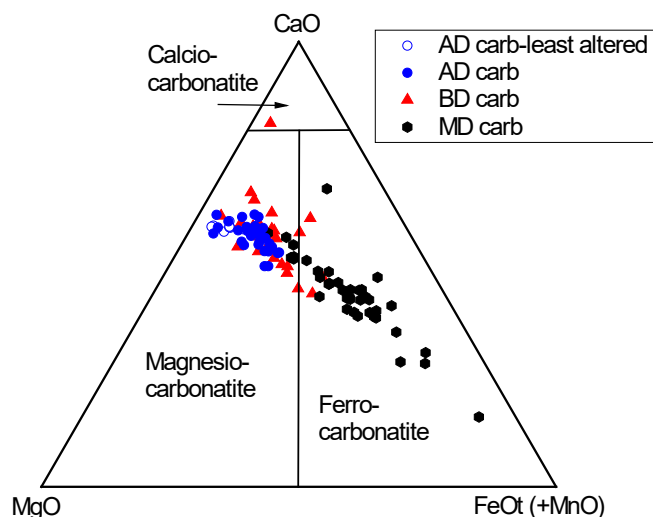


Fig. 10. Ternary diagram of major element concentration data for Elk Creek alkaline complex carbonatite units after Woolley and Kempe (1989). AD Carb = apatite-dolomite carbonatite; MD Carb = magnetite-dolomite carbonatite; BD Carb = barite-dolomite carbonatite.

(1.7% Fe and 0.6 Mn, n = 67). The Fe concentrations of grains of DOL2s are consistently greater than those measured in grains of DOL1s, as are the Mn concentrations. The median values for Fe and Mn in DOL2A in the altered AD carbonatite are 10.3% Fe and 0.7% Mn (n = 8) whereas the median values for Fe and Mn in DOL2B in the MD carbonatite are 14.3 and 1.2%, respectively (n = 62).

Rare earth element concentrations for dolomite (DOL1A) and apatite in the least altered AD carbonatite were determined by LA-ICP-MS (Supplementary data Table 3). The REE patterns of both dolomite and

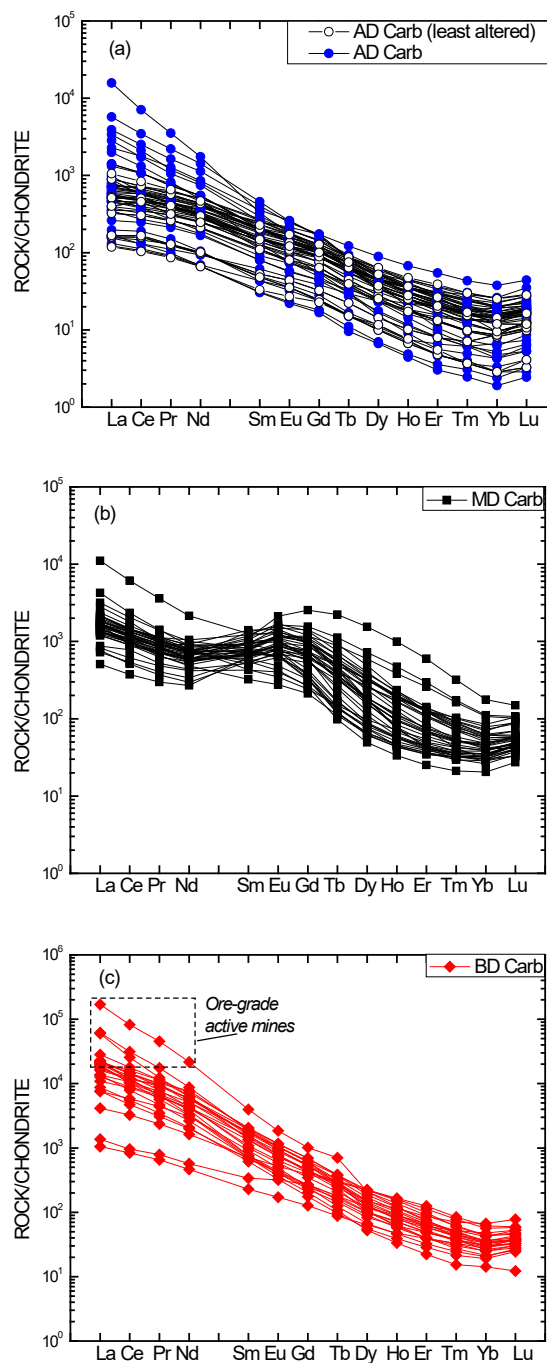
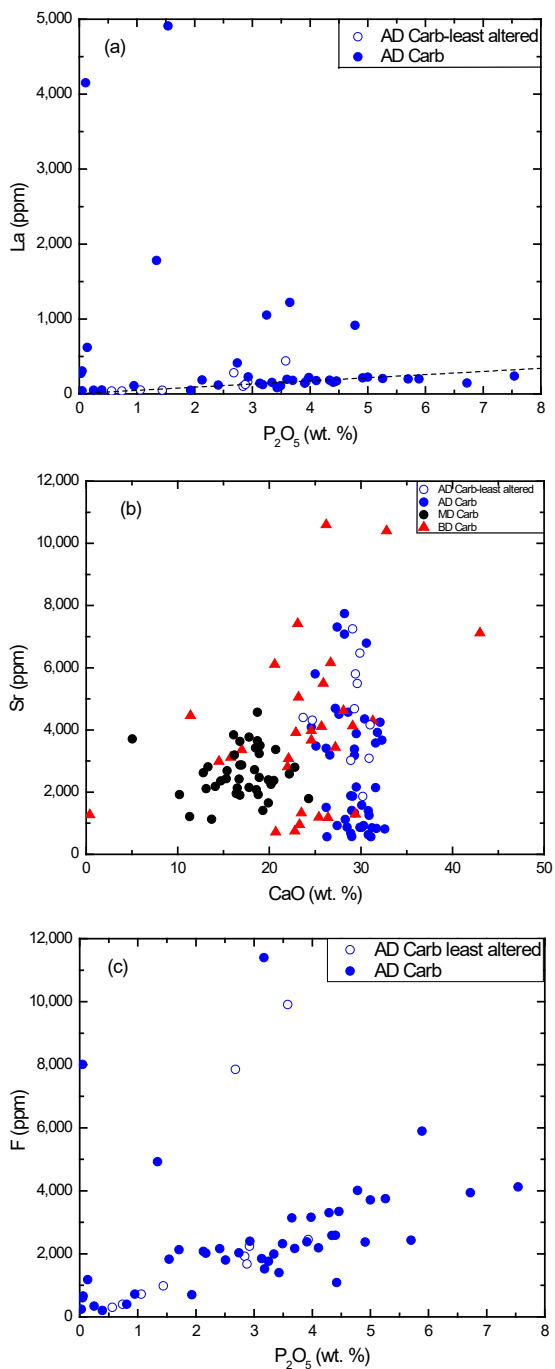


Fig. 11. (a) Chondrite-normalized rare earth element diagram of apatite-dolomite carbonatite samples. (b) Chondrite-normalized rare earth element diagram for magnetite-dolomite carbonatite samples. (c) Chondrite-normalized rare earth element diagram for barite-dolomite BD carbonatite samples. Data normalized to chondrite values of Anders and Ebihara (1982). Data for field for ore-grade samples from active carbonatite-related mines from Fan et al. (2016) and Verplanck et al. (2016); AD Carb = apatite-dolomite carbonatite; MD Carb = magnetite-dolomite carbonatite; BD Carb = barite-dolomite carbonatite.

apatite display light REE enrichment and a negative slope, with the apatite REE concentrations ~100 greater than those measured in dolomite (Fig. 14). Mass balance calculations using P as a proxy for apatite and Mg as a proxy for dolomite suggests that ~60% of the REEs are hosted by apatite and ~40% by dolomite. To determine which mineral controls the middle REE enrichment in the MD carbonatite, laser ablation analysis was undertaken, and the fine-grained dolomites (DOL2B)



**Fig. 12.** (a) Diagram displaying variation in lanthanum (La) and phosphate ( $P_2O_5$ ) in apatite-dolomite carbonatite samples. (b) Diagram displaying variation in strontium (Sr) and calcium (CaO) in carbonatite samples. (c) Diagram displaying variation in fluorine (F) and phosphate ( $P_2O_5$ ) in apatite-dolomite carbonatite samples.

were identified as having middle REE enriched patterns (Fig. 15a and b). Slight differences in the peak enrichment in the patterns of dolomites from different samples were observed.

#### 4.6. Isotopic results

Whole rock sample Nd and Sr isotopic data are presented in [Supplementary data Table 4](#) and mineral C, O, and Sr isotopic data is presented in [Supplementary data Table 5](#). Most of the samples analyzed for Sr and Nd isotopic compositions were splits of the 10-foot composite

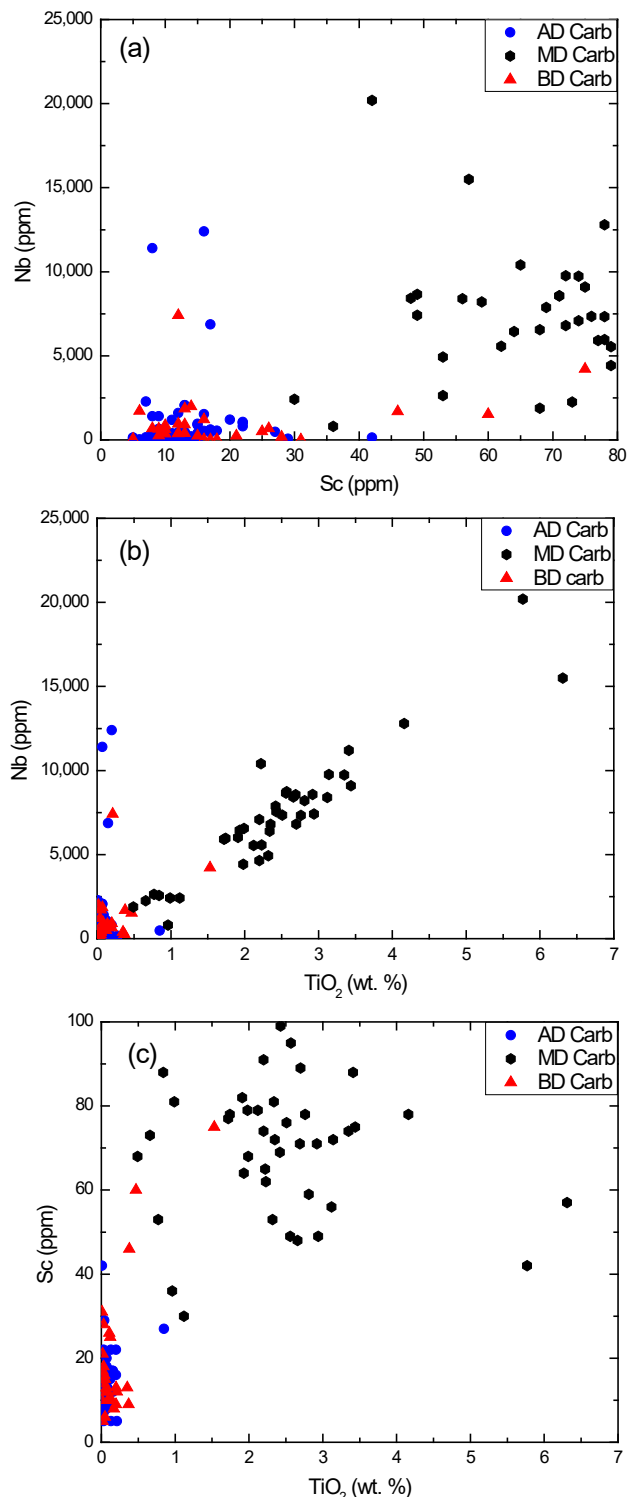


**Fig. 13.** Diagrams displaying variation of a) niobium (Nb) and scandium (Sc); b) niobium (Nb) and titanium ( $TiO_2$ ); and c) scandium (Sc) and titanium ( $TiO_2$ ) for Elk Creek carbonatite samples. AD = apatite-dolomite carbonatite; MD = magnetite-dolomite carbonatite; BD = barite-dolomite carbonatite.

pulp samples. These were the initial set of samples collected to gain insight into the chemical composition of the major lithologic units. The large variation in the Sm/Nd ratios of the carbonatite samples allows for an isochron age to be determined,  $571 \pm 7$  Ma; Fig. 16. Samples that are moderately to extensively altered still plot along the isochron. Using this age, the initial Nd isotopic composition of the Elk Creek carbonatite

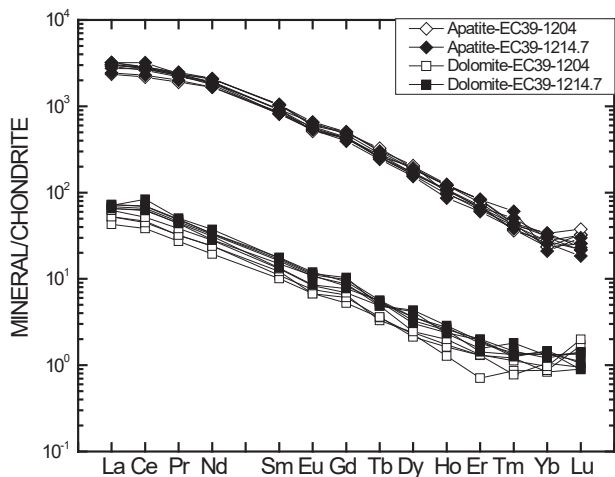


**Fig. 14.** Chondrite-normalized rare earth element diagram displaying rare earth element patterns for apatite and dolomite in two samples of apatite-dolomite carbonatite. Data normalized to chondrite values of [Anders and Ebihara \(1982\)](#).

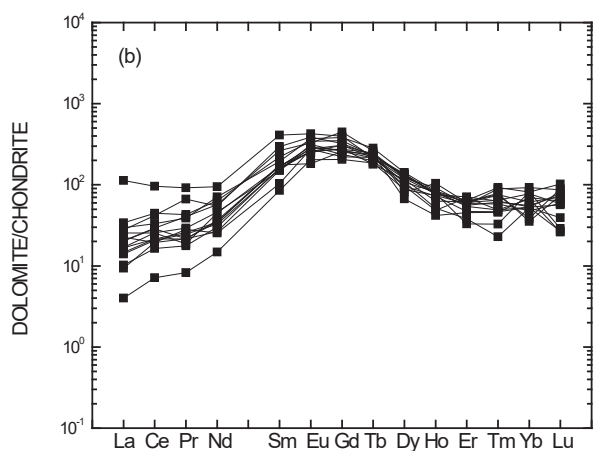
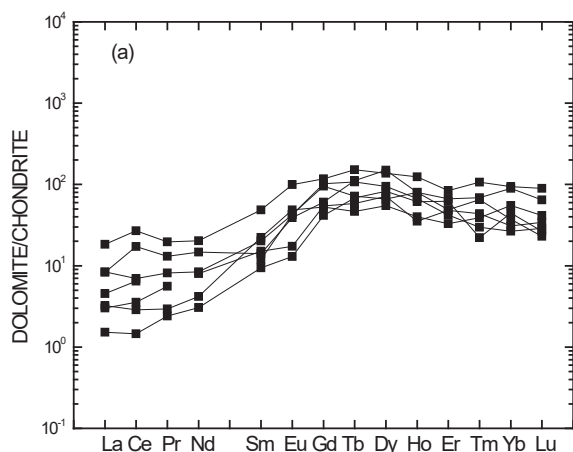


**Fig. 15.** Chondrite-normalized rare earth element diagram dolomite from magnetite-dolomite carbonatite samples. Data normalized to chondrite values of [Anders and Ebihara \(1982\)](#).

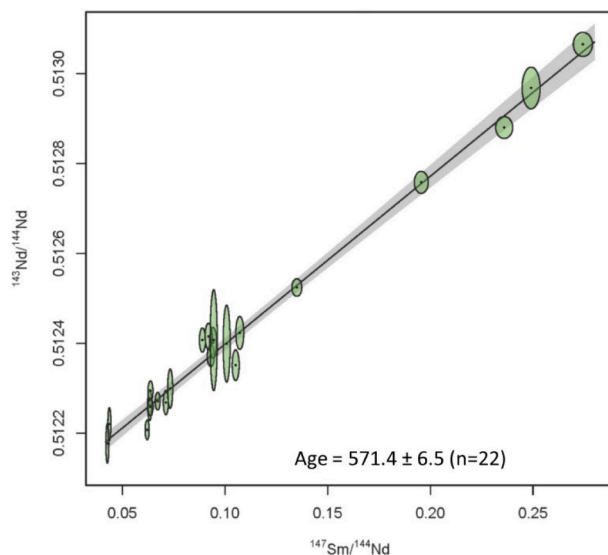


**Fig. 16.** Graph displaying measured  $^{143}\text{Nd}/^{144}\text{Nd}$  versus  $^{147}\text{Sm}/^{144}\text{Nd}$  for Elk Creek carbonatite and syenites. Age calculated from best-fit regression =  $571.4 \pm 6.5$  Ma.  $^{143}\text{Nd}/^{144}\text{Nd}$  of y-intercept = 0.51202.

samples can be calculated, and the  $\epsilon_{\text{Nd}}(T) = 1.9$  to 3.4. The  $\epsilon_{\text{Nd}}(T)$  of the four samples of altered syenite ranges from 1.1 to 2.9.

Unlike the Nd isotopic data, the Sr isotopic data does not plot along a linear array and cannot be used to calculate an isochron age (Fig. 17). Using the 571 Ma age, the calculated  $\text{Sr}_i$  isotopic ratios for the rock samples range from 0.7027 to 0.7075. The AD carbonatite samples range from 0.70270 to 0.70330, with the subset of AD carbonatite samples with coarse-grained dolomite (DOL1A) and apatite groups at low Sr isotopic compositions, 0.70270 to 0.70290 (Fig. 18). The  $\text{Sr}_i$  of the MD carbonatite samples (5 samples) ranges from 0.70395 to 0.70500, with the samples that display iron oxidation having greater than 0.7045 values. The initial  $^{87}\text{Sr}/^{86}\text{Sr}$  ratios of the two relatively fresh BD carbonatite samples are 0.70395 to 0.70413; a BD carbonatite sample overprinted by extensive iron oxidation alteration has an initial  $^{87}\text{Sr}/^{86}\text{Sr}$  ratio of 0.70522. The  $\text{Sr}_i$  of the four samples of altered syenite ranges from 0.70344 to 0.70413. Two 10-foot composite core samples with the highest Sr initial isotopic compositions (0.70569 and 0.70747) contain a mixture of lithologies including younger mafic dikes. These samples are not included in carbonatite discussions that follow because

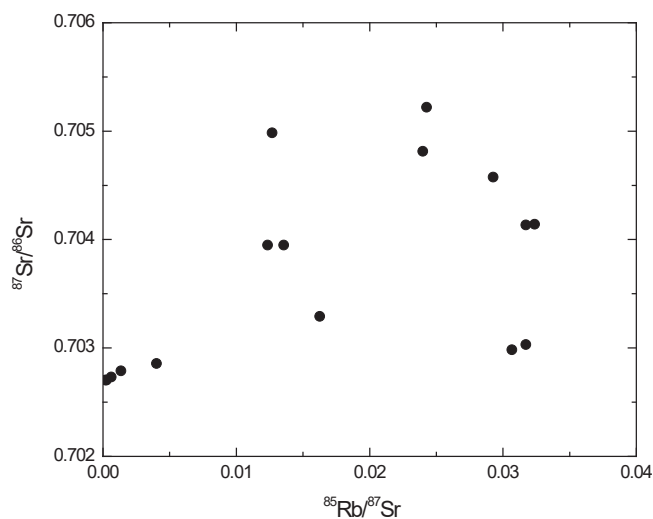


**Fig. 17.** Graph displaying measured  $^{87}\text{Sr}/^{86}\text{Sr}$  versus  $^{85}\text{Rb}/^{87}\text{Sr}$  for Elk Creek carbonatite samples.

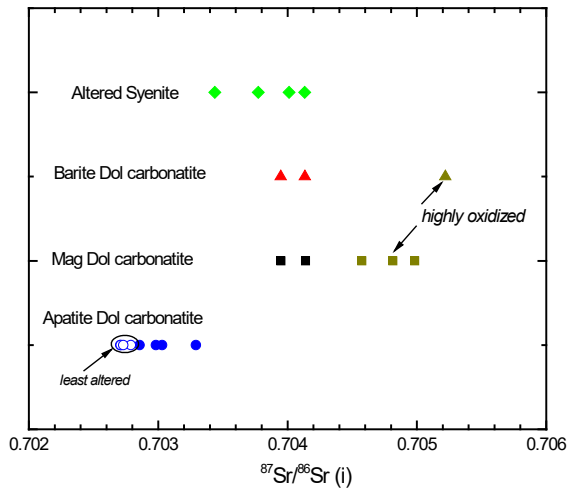


**Fig. 18.** Diagram displaying  $^{87}\text{Sr}/^{86}\text{Sr}(i)$  ratio for Elk Creek samples by lithological unit.

of the unknown age of the younger mafic dikes. Overall, the range in Sr isotopic compositions presented here are similar to the results reported in [Brookins et al. \(1975\)](#) for carbonatite samples (0.7030 to 0.7056).

The  $\delta^{13}\text{C}$  and  $\delta^{18}\text{O}$  values of a set of dolomites were determined. These samples were drilled from billets using a microdrill such that samples from complex lithologies, DOL2 with DOL1, may not represent 100% of a mineral phase. These samples display a moderate range of  $\delta^{13}\text{C}$  values ( $-4.4$  to  $-1.2\text{‰}$ ) and a large range of  $\delta^{18}\text{O}$  values (8.8 to 23.0‰; [Fig. 19a](#)). Four coarse-grained DOL1A samples plot within or just above the primary igneous carbonate field (PIC) defined by [Deines \(1989; Fig. 19a\)](#). The PIC field is designated from carbonate minerals in carbonatites unaffected by alteration and is representative of the mantle source composition ([Broom-Fendley et al., 2017b](#)). Of these samples, two dolomite samples are from the fresh AD carbonatite, and two samples from the AD and BD carbonatites that also contain DOL2. These samples have the lowest  $\delta^{18}\text{O}$  values. The dolomites with the highest  $\delta^{18}\text{O}$  values (22.3 and 23.0‰) also have the highest  $\delta^{13}\text{C}$  values ( $-1.18$  and  $-1.45\text{‰}$ ). These dolomites are from a BD carbonatite sample that is overprinted by extensive iron oxidation. Three dolomite samples from a single AD carbonatite sample that primarily contains DOL2 have a range of  $\delta^{18}\text{O}$  and  $\delta^{13}\text{C}$  values; the  $\delta^{18}\text{O}$  ranging from 18.0 to 21.2‰ and the  $\delta^{13}\text{C}$  ranges from  $-2.32$  to  $-3.25\text{‰}$ . Dolomites from three carbonatite samples that contain both DOL1 and DOL2 plot in a field between the PIC field and the three DOL2 from previously mentioned AD carbonatite.

Powders from a subset of these dolomite samples were also analyzed for their strontium isotopic compositions; their  $^{87}\text{Sr}/^{86}\text{Sr}$  ratios vary from 0.70270 to 0.70526 ([Fig. 19a](#)). The sample of DOL1A from the fresh AD carbonatite sample had the lowest  $^{87}\text{Sr}/^{86}\text{Sr}$  value (0.70270), whereas dolomite from the iron oxidation altered sample had the highest  $^{87}\text{Sr}/^{86}\text{Sr}$  value (0.70526). A sample comprising primarily of DOL1 from a BD carbonatite had a  $^{87}\text{Sr}/^{86}\text{Sr}$  value of 0.70319 and a dominantly DOL2 dolomite from the same BD carbonatite sample had a  $^{87}\text{Sr}/^{86}\text{Sr}$  value of 0.70332. Two DOL2 dolomites from the AD carbonatite that is primarily composed of DOL2 had  $^{87}\text{Sr}/^{86}\text{Sr}$  values of 0.70334 and 0.70343.

## 5. Discussion

### 5.1. Relative ages of the Elk Creek carbonatite lithologies

The Elk Creek carbonatite intruded alkaline silicate units that have

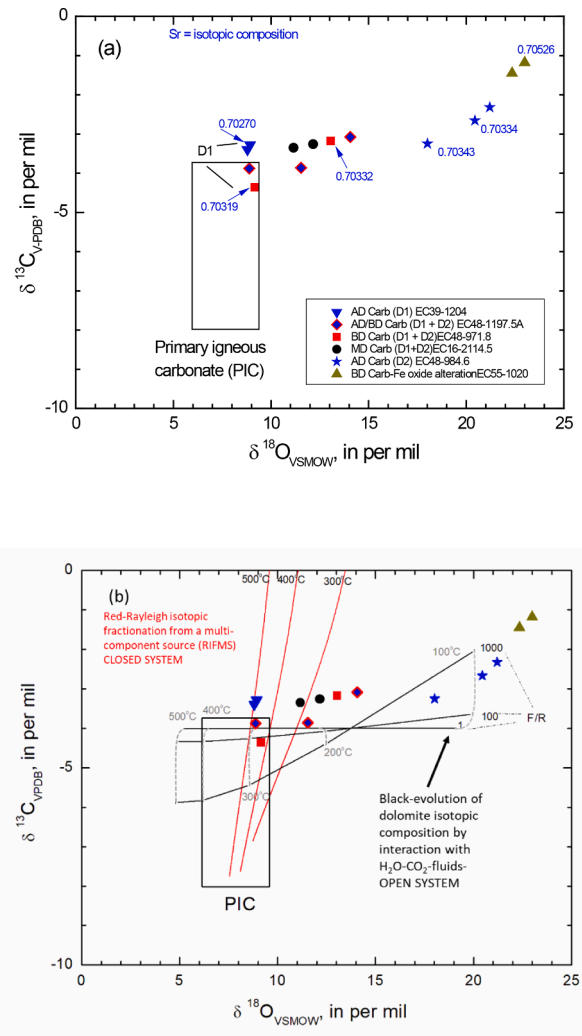


**Fig. 19.** (a) Oxygen and carbon isotope compositions of dolomites from the Elk Creek carbonatite. Primary igneous carbonate (PIC) field from [Deines \(1989\)](#) and overlaps fields from [Taylor et al. \(1967\)](#) and [Demény et al. \(2004\)](#). Plot includes strontium isotopic composition of a subset of dolomites analyzed for C and O isotopic compositions in blue. (b) Oxygen and carbon isotope compositions of dolomites from the Elk Creek carbonatite with Rayleigh fractionation and dolomite-fluid interaction modeling results. C-O isotopic data with modeling results of Rayleigh isotopic fractionation from a multi-component source (RIFMS) displaying the trend in isotopic composition of dolomite shown with the closed-system Rayleigh-type fractionation of the carbonatite with its exsolved fluid at 500 °C, 400 °C and 300 °C (red lines). The fluid was modelled as having source  $\delta^{13}\text{C}$  and  $\delta^{18}\text{O}$  values are  $-4\text{‰}$  and  $8.5\text{‰}$ , and an initial molar  $\text{CO}_2/\text{H}_2\text{O}$  ratio of 0.41. Black lines depict the modeling results of the evolution of dolomite isotopic composition by interaction with  $\text{H}_2\text{O}-\text{CO}_2$  fluids ( $\text{CO}_2/\text{H}_2\text{O} = 1/1000$ ) with in the fluid-rock isotope exchange model from [Santos and Clayton \(1995\)](#). The fluid was modelled with  $\delta^{13}\text{C} = -4\text{‰}$  and  $\delta^{18}\text{O} = 3\text{‰}$ , and the initial isotopic composition of the dolomite was  $\delta^{13}\text{C} = -4$  and  $\delta^{18}\text{O} = 9.5$ . The fluid-rock ratio varies from 1 to 1000, and temperature varies from 100 to 400 °C. The fractionation factors were determined using the thermodynamic data of [Richet et al. \(1977\)](#), [Chacko et al. \(1991\)](#), and [Horita \(2014\)](#).

been fenitized. Drill core penetrated the silicate lithologies along the margin of the carbonatite, and clasts of alkaline silicate units are included in the carbonatite, consistent with the carbonatite being younger than the alkaline silicate units. The  $\epsilon_{\text{Nd}}(T)$  of four alkaline silicate samples (1.1 to 2.9) overlap the range for the carbonatite, suggesting a common source. The alkaline silicate rock samples have been metasomatized, reflected in the depletion of  $\text{SiO}_2$  (27.9 to 36.3 wt%) and

enrichment in CaO, K<sub>2</sub>O, and Na<sub>2</sub>O, typical of alkali metasomatism associated with carbonatites (Woolley, 1982; Elliott et al., 2018).

The primary carbonate mineral in the Elk Creek carbonatite is dolomite; calcite-rich lithologies have not been identified. Although this feature is not unique, most carbonatites contain calcite-rich portions (Woolley, 1982; Gittins, 1989; Le Bas, 1999). On the carbonatite ternary diagram (Fig. 10), the AD carbonatite and MD carbonatite samples form a trend towards the iron endmember, with the least altered AD carbonatite samples located at the start of the trend. The evolution from a Mg-rich carbonatite to an Fe-rich carbonatite is a typical feature of carbonatite systems; recent experimental results display similar evolution (Anenburg et al., 2020). Clasts of DOL1 (DOL1B), the primary dolomite in the early, fresh AD carbonatite, are found in the MD carbonatite and are surrounded by a finer-grained dolomite (DOL2B) (Fig. 7). The clasts appear to be fragments of AD carbonatite within the MD carbonatite, such that the MD carbonatite is younger than the AD carbonatite. The BD carbonatite, the unit with the highest REE values, is clearly younger than the other two carbonatite lithologies because veins of BD carbonatite cut the other two units. Mineralized carbonatites typically display late-stage Ba and REE enrichment (Verplanck et al., 2016), and the Elk Creek carbonatite is no exception.

One important observation is that the Nd isotopic data for all lithologies plot along a linear array and form an isochron with an age of  $571 \pm 7$  Ma. To form a linear array suggests that the Nd in all the units came from the same source and the units are approximately contemporaneous. The REEs may have been mobilized during hydrothermal alteration, but this event would have to be contemporaneous with, or immediately following, emplacement. The Sm/Nd ratio and <sup>143</sup>Nd/<sup>144</sup>Nd values of all samples have evolved in a closed system since cessation of carbonatite emplacement and related hydrothermal alteration. The initial  $\epsilon_{Nd}(T)$  values for the carbonatites range from 1.9 to 3.4 with a median value of 2.4. This is consistent with a mantle source of the carbonatite magma. Similar isotopic compositions have been noted for other mineralized carbonatites, including Iron Hill (USA), Kangankunde (Malawi), and Khibina (Russia) (Zaitsev et al., 2002; Premo and Lowers, 2013; Verplanck et al., 2016).

## 5.2. Magmatic and hydrothermal features

Textural, chemical, and C, O, and Sr isotopic data reveal that the Elk Creek carbonatite underwent a complex evolution. Other studies of mineralized carbonatites have observed similar features, including complex textural relationships, enrichment in both light and middle/heavy REEs, and variations in C, O, and Sr isotopic ratios. Many of these features can be attributed to fluids primarily derived from an evolving carbonatite magma (Williams-Jones et al., 2012; Dietzel et al., 2019).

Carbonatite magmas may contain significant amounts of water (Keppler, 2003) with the fraction of water increasing as anhydrous carbonate minerals crystallize. In the latter stages of evolution, an aqueous fluid phase can exsolve (Bühn, 2008; Anenburg et al., 2020). This carbonatite-derived orthomagmatic fluid has been termed “carbothermal” fluid (Mitchell, 2005). The presence of fenitized wall rock adjacent to carbonatites is evidence of the hydrothermal systems associated with carbonatites. Elliott et al. (2018) reviewed the state of knowledge of fenites and highlighted that 1) the alteration is generally formed by multiple pulses of fluids, 2) brecciation is typical and may provide pathways for fluid flow, and 3) although fluids that contain a variety of constituents that include Na, K, REEs, Nb, F, Cl, CO<sub>2</sub>, H<sub>2</sub>O, and HCO<sub>3</sub><sup>-</sup> tend to move from the carbonatite outward, there are examples of the transport of elements, principally Si, from the country rock to the carbonatite.

The AD carbonatite has a range in texture and chemistry. Chemically, the fresh, medium to coarse grained AD carbonatite plots at the starting point of the carbonatite trend on the carbonatite ternary diagram (Fig. 10) and has low and LREE-enriched REE patterns (Fig. 11a). The  $\delta^{13}C$ ,  $\delta^{18}O$ , and <sup>87</sup>Sr/<sup>86</sup>Sr values are consistent with this subunit

being of primary igneous origin that has mantle affinities. These features are consistent with the unaltered AD carbonatite being a relatively early crystallized carbonatite. In addition, the presence of ovoid apatite crystals and subhedral to euhedral zoned pyrochlore in this subunit support a primary magmatic origin (Le Bas, 1999). Dolomite within this unit is LREE-enriched and contains relatively little Fe and Mn. The  $\delta^{13}C$ ,  $\delta^{18}O$ , and <sup>87</sup>Sr/<sup>86</sup>Sr values of DOL1 from the unaltered AD carbonatite plot in primary igneous carbonate and the mantle fields. These elemental concentrations and isotope ratios are also similar to those observed in Type 1 calcites within carbonatites from the Miaoya deposit (China) that were shown to be of primary igneous origin (Ying et al., 2020). Overall, the REE content of this unit is relatively low, except where late-stage REE minerals occur primarily in vugs and cavities. Although apatite crystallization takes up a fraction of the REEs, the REE content of the residual magma likely increases because of the simultaneous crystallization of REE-poor phases, such as dolomite (Hornig-Kjarsgaard, 1998; Ionov and Harmer, 2002).

The AD carbonatite in closer proximity to the MD and BD carbonatite and breccias displays a less equigranular texture and contains dolomite (DOL2A) that is fine-grained. These dolomites have higher Fe and Mn contents than DOL1s and may surround and invade dolomite with low Fe and Mn content (Fig. 3b). Fluid inclusion studies by Bühn and Rankin (1999) documented elevated Fe and Mn concentrations in the fluids expelled from a carbonatitic magma and concluded that these two elements would be removed from the fluid relatively early. Fine-grained quartz can occur within masses of fine-grained dolomite. These features are consistent with this portion of the AD carbonatite undergoing recrystallization during metasomatic activity (Trofanenko et al., 2016; Ying et al., 2020).

Vugs and cavities within the AD carbonatite are partially filled with fine-grained REE minerals including parisite, synchysite, bastnäsite, and monazite as well as quartz and iron oxide, with occasional fluorite and dolomite (Fig. 5a and b). Examples of skeletal remains of apatite have also been observed. Some pyrite within the carbonatite units is also corroded and embayed. These features are evidence of metasomatic activity by fluids of varying compositions, and since REE minerals are associated with these textures, it suggests that the REE mineral phases crystallized during these events.

The MD carbonatite occurs near the center of the carbonatite, is younger than the AD carbonatite, and is brecciated. Laser ablation analyses of minerals in this lithology show that the fine-grained dolomite (DOL2B) has a middle REE-enriched pattern, and this accounts for the whole rock REE pattern. These dolomites are also enriched in Fe and Mn compared to DOL1s. Although carbonatites are generally characterized by enrichment in LREE, recent studies have documented zones of middle and heavy REE enrichment (Chakhmouradian et al., 2016; Broom-Fendley et al., 2016b, 2017b; Andersen et al., 2016, 2017; Ranta et al., 2018; Ying et al., 2020). These studies attribute this pattern to hydrothermal transport and fractionation of the REEs, but there is debate on the actual mechanism controlling REE fractionation, which is discussed in the following section. Within this unit are vugs and cavities with fine-grained REE phases, along with and barite, dolomite, quartz, iron oxide, and a thorium phase. These assemblages suggest multiple fluid pulses with a range in compositions.

The barite dolomite carbonatite occurs as late-stage veins and has extreme LREE enrichment. The pervasive alteration adjacent to most veins (Fig. 8c) is evidence of the high fluid content. Fine-grained barite, dolomite, and quartz also occur surrounding coarse dolomite. The REE enrichment and association with barite and quartz in late stages of carbonatite complex is observed in other deposits, such as the Fen complex (Norway) and Maoniuping deposit (China) and is usually attributed to deposition from evolved hydrothermal fluids (Mariano, 1989a, 1989b; Xie et al., 2015; Dahlgren, 2019; Dietzel et al., 2019). We interpret the BD carbonatite to be derived from hydrothermal fluids because it is the youngest unit, contains classic carbonatite hydrothermal mineral associations, and has extensive alteration halos that

surround most veinlets.

Fluorite is not a common mineral in the Elk Creek carbonatites, but in this study, fluorite veinlets were observed in the BD carbonatite and occasionally in the AD carbonatite. These late fluorite occurrences suggest a F-rich fluid was present but not a major feature.

Breccias are identified within all AD and MD carbonatite units but are most prevalent within and adjacent to the MD carbonatite. Of note most breccias primarily contain one type of clast, and the MD carbonatite is the most common lithology. Matrix material is variable but usually consists of either dolomite, magnetite, and quartz or dolomite, barite, and quartz. Breccias are common in many ore deposits (Sillitoe, 1985; Jebrack, 1997), including mineralized carbonatites (for example Xie et al., 2009; Liu et al., 2015; Nadeau et al., 2018; Verplanck et al., 2016; Elliott et al., 2018) and are the result of an increase in fluid pressure culminating with failure. The range in clast and matrix composition of the breccias within the Elk Creek carbonatite point to multiple brecciation events with differing fluid compositions.

### 5.3. Nature of hydrothermal fluids-sources and evolution

Coupling the elemental, petrographic, and isotopic data provides insight into the nature of the hydrothermal fluids. The Nd isotopic data are consistent with all the Nd being derived from the same source, and no significant post-emplacement fractionation between Nd and Sm occurred because the Nd isotopic data form a linear array (Fig. 16). In contrast  $\delta^{13}\text{C}$ ,  $\delta^{18}\text{O}$ , and  $^{87}\text{Sr}/^{86}\text{Sr}$  data display a range in values and can be used to constrain the nature of processes affecting the evolution of the carbonatite (Deines, 1989; Santos and Clayton, 1995; Trofanenko et al., 2016; Broom-Fendley et al., 2017b; Ying et al., 2020). The freshest AD carbonatite samples have the lowest initial  $^{87}\text{Sr}/^{86}\text{Sr}$  values (0.70270–0.70286), whereas the AD carbonatite samples with hydrothermal DOL2A, (greater Fe and Mn contents), tend to have slightly higher initial  $^{87}\text{Sr}/^{86}\text{Sr}$  values (0.70298 to 0.70330). The slight increase in initial  $^{87}\text{Sr}/^{86}\text{Sr}$  values observed in the more altered AD carbonatite is consistent with Sr derived from a mantle source or addition of more radiogenic Sr to the magma.

Whole rock initial  $^{87}\text{Sr}/^{86}\text{Sr}$  values of those BD and MD carbonatites that comprise significant hydrothermal mineral phases but lack extensive iron oxidation have a similar range (0.70395 to 0.70414), whereas oxidized samples of these rocks have higher initial  $^{87}\text{Sr}/^{86}\text{Sr}$  values (0.7046–0.7052) (Fig. 18). Initial  $^{87}\text{Sr}/^{86}\text{Sr}$  values of fenitized syenite samples overlap this range (0.7034 to 0.7041). Overprinting by iron-oxidizing fluids appears to be the final event; it is unclear if this occurred late in the carbonatite evolution or was a younger event. The less altered MD and BD carbonatite samples with initial  $^{87}\text{Sr}/^{86}\text{Sr}$  values ranging from 0.7034 to 0.7041 is evidence that the hydrothermal fluid was in part derived from a more radiogenic source. Fluids derived from interaction with the Precambrian-age granites and gneisses in the country-rock are a likely source because of their proximity and the observed fenitization. At 571 Ma, the strontium isotopic composition of the Precambrian wall rock would have a significantly more radiogenic composition than orthomagmatic fluids derived from the carbonatite.

The Sr isotopic data can be coupled with the  $\delta^{13}\text{C}$  and  $\delta^{18}\text{O}$  values to aid in constraining the source of the metasomatic fluids. The  $\delta^{13}\text{C}$  and  $\delta^{18}\text{O}$  values of DOL1s from the AD and BD carbonatites plot within the primary igneous carbonatite field (Fig. 19a). The  $\delta^{13}\text{C}$  and  $\delta^{18}\text{O}$  values obtained from other dolomites (DOL2A and B) and from the AD, MD, and BD carbonatites plot along a curvilinear trend with increasing  $\delta^{13}\text{C}$  and  $\delta^{18}\text{O}$  values (Fig. 19a). Processes that can fractionate C and O isotopes in an evolving carbonatite include closed system Rayleigh crystal fractionation or fluid-rock interaction (Andersen, 1987; Trofanenko et al., 2016; Broom-Fendley et al., 2017b; Andersen et al., 2019; Ying et al., 2020). Closed system Rayleigh crystal fractionation occurs as the magma cools and dolomite crystallizes. The isotopes of C and O can fractionate as the lighter isotope is preferentially incorporated in dolomite (Pineau et al., 1973; Ray and Ramesh, 2000). Fig. 19b displays

calculated C-O isotopic fractionation for dolomite crystallizing at 500, 400, and 300 °C. The C-O isotopic composition of DOL1 samples plot on or near the calculated compositions for Rayleigh fractionation, such that DOL1's isotopic composition is consistent with primary igneous dolomite crystallizing from an evolving carbonatite magma.

Most other samples have greater  $\delta^{13}\text{C}$  values for a given  $\delta^{18}\text{O}$  value, and are evidence that other processes were at work. The C and O isotopic composition of dolomite can be affected by interaction with external fluids. Following the method outlined in Santos and Clayton (1995) and utilized in Ying et al (2020), we modelled the C and O isotopic variation resulting from dolomite interacting with  $\text{H}_2\text{O}-\text{CO}_2$ -fluids at temperatures from 400 to 100 °C (Fig. 19b). Most of the dolomite data lies in this field consistent with the fluid being a mixture of fluid derived from the carbonatite and fluid derived from the country rock. The observed increase in Sr isotopic composition is consistent with a contribution from hydrothermal fluids with more radiogenic strontium resulting from circulation through the country rock. The presence of quartz in late-stage cavities is also consistent with late-stage input of silica derived from fluids that interacted with silicic country rock. The C-O isotopic composition of dolomite from the most altered sample, plot to the right of the model results indicating that it likely formed late in the sequence, or this alteration could be related to a younger event.

Most mineralized carbonatites contain evidence for multiple fluid compositions and hydrothermal events. Such evidence has been reported at Fen (Andersen, 1986; Dietzel, et al., 2019), Kangankunde (Wall and Mariano, 1996; Broom-Fendley et al., 2017b), Mauniuping (Xie et al., 2015), and Bayan Obo (Smith and Henderson, 2000; Song et al., 2018). Unraveling the magmatic-fluid evolution is, therefore, challenging. Further complicating interpretation of the role of fluid composition on REE mobility is lack of consensus among experimental studies. Most investigations point to volatiles in the fluid as primary control of REE fate and transport, but two recent studies highlight the potential importance of K, Na, and Si (Anenburg et al., 2020; Cui et al., 2020). A third recent study, Louvel et al. (2022), presents experimental results that show carbonate complexation in alkaline fluids can not only transport REEs but also fractionate light and heavy REEs. Our study does not have adequate information to resolve these issues but can provide some insight.

Two units in the Elk Creek carbonatite are important hosts to REE mineralization, the magnetite-dolomite carbonatite is enriched in middle/heavy REEs, in particular Dy, and the barite-dolomite carbonatite is enriched in light REEs. Both these units have been affected by hydrothermal overprinting. Other mineralized carbonatite studies have reported zones of middle and heavy REE enrichment including Fen (Norway), Bear Lodge (USA), Tundulu (Malawi), and the Huanglongpu area (China) (Andersen, 1986; Broom-Fendley et al., 2016b, 2017a; Andersen et al., 2016, 2017; Smith et al., 2018). In these studies, the HREE-enriched zone is outward relative to the LREE enrichment, generally on the margins of the carbonatite or in the adjacent country rock. In the case of the Elk Creek carbonatite, the MREE/HREE-enriched MD carbonatite occurs near the center of the carbonatite and formed prior to the LREE-enriched BD carbonatite; thus, there is temporal variation instead of a spatial variation. The host mineral for the MREE enrichment is the fine-grained hydrothermal dolomite (Fig. 15). Two scenarios could lead to the middle/heavy REE patterns of the hydrothermal dolomite in the MD carbonatite: 1) either the fluid from which the dolomite precipitated was enriched in middle/heavy REEs and there was no preferential complexing agent in the fluid to fractionate the REEs or 2) the light REEs in the fluid were more strongly complexed thus retarding their partitioning into the secondary dolomite and thus forming a middle/heavy REE-enriched secondary dolomite. We believe the second scenario is more likely in this case because crystallization of the apatite and dolomite in the AD carbonatite did not deplete the residual magma in LREEs but likely enhanced the REE concentrations. Carbonatite magmas are characterized by extreme LREE-enrichment, and the REE composition of early formed minerals, including calcite,

dolomite, and apatite, reflect the overall REE pattern of the magma and do not fractionate it, unless REE-rich accessory phases crystallize (Hornig-Kjarsgaard, 1998).

Possible ligands in the hydrothermal fluid that complex with REEs include  $\text{Cl}^-$ ,  $\text{CO}_3^{2-}$ ,  $\text{F}^-$ ,  $\text{OH}^-$ ,  $\text{PO}_4^{3-}$ , and  $\text{SO}_4^{2-}$ . Overall, fluorine concentrations in the EC carbonatite are low, and recent work has shown that  $\text{F}^-$  is not likely the primary control of REE complexation in carbonatites (Migdisov and Williams-Jones, 2014; Migdisov et al., 2016). Phosphate tends to have a low solubility in low-temperature fluids and, if present, leads to precipitation of monazite or other REE-phosphate phases (Louvel et al., 2015; Migdisov et al., 2016).  $\text{OH}^-$  and  $\text{SO}_4^{2-}$  are possible ligands, but experimental work shows that there is minimal variation in the strength of complexation with increasing atomic number across the REEs (Migdisov et al., 2016); thus, these ligands would not lead to the observed REE fractionation. This leaves  $\text{Cl}^-$  and  $\text{CO}_3^{2-}$  as the remaining possible ligands. Although we have not undertaken a fluid inclusion study at Elk Creek, other studies of fluid inclusions associated with carbonatites have shown that fluids may be acidic and then chloride would be the dominant ligand (Migdisov et al., 2016). Numerous cavities in the MD carbonatite and skeletal apatite in the AD carbonatite are consistent with interaction with an acidic fluid. Fluid inclusion studies of carbonatites document elevated NaCl concentrations, in excess of 10 wt% (Banks et al., 1994; Smith and Henderson, 2000; Williams-Jones et al., 2000; Bühn et al., 2002). Furthermore, modeling results show that chlorine is likely the dominant ligand in acidic fluids (Perry and Gysi, 2018). Experimental studies by Migdisov et al. (2009) showed that at 250 °C or greater, there is a systematic decrease in the strength of complexation with increasing mass for REECl complexes, resulting in the relationship that LaCl complexes are more stable than LuCl complexes. With REE-chloride species having stronger LREE complexation (Migdisov et al., 2016), the HREE would preferentially be incorporated into the hydrothermal dolomite and lead to the observed REE pattern of the dolomite in the MD carbonatite.

Louvel et al. (2022) present a case for hydrothermal fluids associated with carbonatites being at least in part circumneutral to alkaline in composition. They point out that 1) fenites surrounding carbonatites document alkaline- and carbonate-rich hydrothermal fluid circulation, and 2) the presence of late-calcite veining associated with many carbonatites suggests a circumneutral to alkaline environment. At Elk Creek, calcite veining does not occur, but hydrothermal dolomite is present as well as fenitized blocks of early alkaline intrusive lithologies. Thus, we cannot discount the possibility that alkaline fluids played a role at Elk Creek. The new experimental results presented in Louvel et al. (2022), show that carbonate complexes can also fractionate REEs at temperatures between approximately 350 and 500 °C. Specifically, in this temperature range La was more soluble than Gd and Yb, which represent middle and heavy REEs respectively, in  $\text{Na}_2\text{CO}_3 \pm \text{NaF}$  fluids. Similar to the behavior of Cl in an acidic environment, this scenario would promote middle/heavy REE enrichment in the hydrothermal dolomite.

By either mechanism, Cl complexation in an acidic fluid or carbonate complexation in an alkaline fluid, removal of middle/heavy REEs from the fluid would further enhance the light REE enrichment in the residual fluid. Late-stage LREE enrichment at Elk Creek is well documented with the BD carbonatite, occurring as veins that crosscut the other carbonatite units and as flooding or overprinting of earlier carbonatite units. Cavities and vugs are also host monazite and fluorocarbonate mineral phases in all carbonatite units. Fluorine- and phosphate-bearing minerals (bastnäsite, parisite, synchysite, and monazite) have low solubilities such that the presence of F and P should lead to precipitation of the observed LREE mineral phases (Poitrasson et al., 2004; Gysi et al., 2015; Gysi and Williams-Jones, 2015). Fine-grained monazite rimming and along fractures of apatite likely formed in this manner. Although F is generally low in the Elk Creek carbonatite, fluorite veinlets and fracture coatings occur, suggesting the presence of fluorine late in the evolution of the carbonatite. A possible scenario for REE precipitation is with the

REEs being present in one fluid and F and/or P present in another fluid, and upon mixing, the REE minerals bastnäsite, parisite, synchysite, and monazite would form (Williams-Jones et al., 2012). In addition, the overall decrease in temperature late in the evolution of the system would also promote precipitation of these mineral phases.

Within the Elk Creek carbonatite, barite is the most common mineral associated with zones of LREE enrichment. The close association of LREE enrichment with barite is observed elsewhere including, Bayan Obo, Maoniuping, Mountain Pass, and Fen. In their review of carbonatite mineralization, Verplanck et al. (2014) noted the strong correlation of Ba and La in world-class REE deposits. Experimental work by Migdisov et al. (2006), documented limited solubility of REEs in sulfate-bearing fluids at hydrothermal temperatures, but recent work by Cui et al. (2020) showed that in the presence of silica, fluids can contain significant higher concentrations of sulfate and transport REEs, based on experiments carried out at ~250 and 400 °C. At Elk Creek we observe the association of barite, REE phases, and quartz (Fig. 2f). This suggests that sulfate may be an important complexing agent. Experimental and modelling work has shown that sulfate may become the more dominant ligand than chloride in near-neutral pH fluids (Migdisov et al., 2016). If the fluid was acidic, fluid interaction with the carbonate mineral phases, dolomite in this complex, would lead to a pH increase. With the precipitation of barite, sulfate would be removed from the fluid, destabilizing the REE sulfate complexes and promoting REE deposition. In addition, with the formation of quartz, Si would be removed from the fluid limiting the amount of sulfate in solution, and again would lead to the destabilization sulfate complexes and REE deposition. Note that unlike REECl complexation, there is no preferential stability of REE- $\text{SO}_4$  complexation across the REEs, such that no mass dependent fractionation would be observed.

Anenburg et al. (2020) conducted a series of experiments from 1200 °C with 1.5 GPa and to 200 °C and 0.2 GPa using REEs, Cl, F,  $\text{CO}_3$ , and P as well as Ca-Mg-Fe-Si-Na-K. They found that in the alkali-free experiments, the REEs formed carbonate and phosphate minerals, which crystallized in cavities. At Elk Creek, we observe numerous examples of monazite and fluorocarbonate minerals in vugs and cavities. In the experiments with alkalis, the authors concluded that there was increased solubility of the REEs in the late hydrothermal fluid because REEs were found in the quenched phase, suggesting that Na and/or K in fluids may enhance the transport of REEs. At Elk Creek, the lack of substantial late-stage K- or Na- phases suggests that complexation with alkali elements may not have been had a major control on the behavior of the REEs in this setting. In a follow-up manuscript, Anenburg et al. (2021) point out that alkali REE carbonate minerals may form during the late magmatic stage, the “melt-brine” stage, but subsequent hydrothermal overprinting would likely breakdown these minerals. The occurrence of burbankite pseudomorphs at few carbonatite localities is presented as evidence of this process. At Elk Creek, monazite and REE fluorocarbonate minerals appear to have formed directly from a fluid phase and do not show evidence of an earlier formed crystal habit. Thus, we cannot rule out that Na and or K played a role in the REE mineralization, but direct evidence is lacking.

As for the sources of various constituents needed to fulfill the above scenarios, an evolving carbonatite magma may be sufficient, but evidence for the breakdown of primary minerals by hydrothermal fluids is clear. This would lead to the remobilizing some constituents. In places, dolomite, apatite, pyrite, and magnetite are pitted and corroded (Figs. 2d, e, and 6c). Dissolution of these phases would contribute Fe, S, P, Ca, and REEs to the hydrothermal fluid. All of these constituents are found in the minerals that precipitated from these fluids. Experimental studies by Harlov et al. (2002, 2005) and Harlov (2015) demonstrate that breakdown of apatite by metasomatizing fluids that contain significant amounts of HCl and  $\text{H}_2\text{SO}_4$  results in reprecipitation of monazite. As discussed above, the Nd isotopic data suggests that all the Nd was derived from the same source, but this does not preclude the remobilization of Nd from earlier-formed minerals. Other carbonatite-

related ore deposit studies have discussed the potential importance of remobilization of REE from earlier-formed minerals as a source of REEs, with the world-class Bayan Obo deposit as an important example (Downes et al., 2014; Fan et al., 2016; Song et al., 2018; Smith et al., 2000).

## 6. Conclusions and implications

Constraining processes that lead to ore-grade enrichment of REEs in carbonatites is needed for cost-effective mineral exploration. The late-stage, barite-dolomite carbonatite at Elk Creek contains LREE enrichment comparable to world-class carbonatite deposits at Bayan Obo, Maoniuping, and Mountain Pass. Neodymium, strontium, and carbon isotopic data from the Elk Creek complex reveal that the parental magma and REEs were derived from the mantle. Textural and chemical data suggest that hydrothermal processes played an important role in reaching ore-grade enrichment, and strontium, carbon, and oxygen isotopic data provide evidence these fluids were derived, in part, from an external source, likely meteoric water that interacted with the country rock. To evaluate fluid evolution, the C-O isotopic data was modeled. Results indicate that some of the isotopic variation can be accounted for by closed-system Rayleigh fractionation of an evolving carbonatitic magma between 300 and 500 °C, but excursions to heavier  $\delta^{18}\text{O}$  is likely the result of interaction with  $\text{H}_2\text{O-CO}_2$ -fluids at temperatures from 400 to 100 °C. Strontium isotopic compositions of hydrothermal dolomite have higher values compared to early-formed magmatic dolomite, which is consistent with metasomatism by fluids derived from a more radiogenic source, such as the Precambrian-age gneissic wall rock.

Processes likely responsible for ore-grade LREE enrichment at Elk Creek include 1) fractional crystallization that enriched the residual melt in REEs; 2) precipitation of middle/heavy REEs-enriched hydrothermal dolomite, which further enhanced the residual fluid in LREEs; and 3) remobilization of REEs from earlier formed minerals. The REEs are primarily hosted in fine-grained, late-stage, cavity filling minerals that include monazite, bastnaesite, parisite, and synchysite along with barite, dolomite, quartz, and iron oxides. The bulk of the REEs are associated with barite, suggesting that barite precipitation destabilized REE sulfate complexes in the fluid that promoted REE deposition. New insight from recent experimental studies, for example Anenburg et al. (2020), Cui et al. (2020), and Louvel et al. (2022), highlight knowledge gaps in our understanding of the fate and transport of REEs in hydrothermal environments and show that transport mechanisms need further investigation.

Remobilization of REEs by hydrothermal fluids is in part responsible for the observed REE enrichment and may be an important process in forming carbonatite-hosted REE deposits. This has been recognized at Bayan Obo for nearly two decades and has recently been identified at other mineralized carbonatites including Miaoya and the Cummins Range Carbonatite Complex (Downes et al., 2014; Ying et al., 2020). Large carbonatites with evidence of hydrothermal overprinting may be ideal exploration targets because they provide a substantial mass of REEs to be leached and redeposited. Dolomite-rich carbonatites may be a better target than calcite-rich carbonatites because the dolomite mineral structure has less capacity to fit REEs than calcite (Chakhmouradian et al., 2016) leading to a higher fraction of REEs in the residual melt. By- or co-product commodities can enhance an ore deposit. In addition to REE enrichment, the Elk Creek carbonatite contains zones of Nb, Sc, and Ti enrichment. Targeting carbonatites with multi-element enrichment could provide additional revenue as demand for various critical elements increases.

## Declaration of Competing Interest

The authors declare that they have no known competing financial interests or personal relationships that could have appeared to influence

the work reported in this paper.

## Acknowledgements

This work was supported by the U.S. Geological Survey Mineral Resources Program including a Mineral Resources Program External Grant, award number G12AP20052, to authors Farmer and Kettler. We thank M. Joeckel of the Nebraska Geological Survey for facilitating storage of, and access to, the public-domain core samples and legacy data. Dr. Sam Broom-Fendley, Bradley Van Gosen, and an anonymous reviewer are thanked for constructive comments and suggestions. Any use of trade, firm, or product names is for descriptive purposes only and does not imply endorsement by the U.S. Government.

## Appendix A. Supplementary data

Supplementary data to this article can be found online at <https://doi.org/10.1016/j.oregeorev.2022.104953>.

## References

- Anders, E., Ebihara, M., 1982. Solar-system abundances of the elements. *Geochim. Cosmochim. Acta* 46, 2363–2280.
- Andersen, A.K., Clark, J.G., Larson, P.B., Neill, O.K., 2016. Mineral chemistry and petrogenesis of a HFSE(+HREE) occurrence peripheral to carbonatites of the Bear Lodge alkaline complex, Wyoming. *Am. Mineral.* 101, 1604–1623.
- Andersen, A.K., Clark, J.G., Larson, P.B., Donovan, J.J., 2017. REE fractionation, mineral speciation, and supergene enrichment of the Bear Lodge carbonatites, Wyoming, USA. *Ore Geol. Rev.* 89, 780–807.
- Andersen, A.K., Larson, P.B., Cosca, M.A., 2019. C-O stable isotope geochemistry and  $^{40}\text{Ar}/^{39}\text{Ar}$  geochronology of the Bear Lodge carbonatite stockwork, Wyoming, USA. *Lithos* 324–325, 640–660.
- Andersen, T., 1986. Compositional variation of some rare earth minerals from the Fen complex (Telemark, SE Norway): implications for the mobility of rare earths in a carbonatite system. *Mineral. Mag.* 50, 503–509.
- Andersen, T., 1987. Mantle and crustal components in a carbonatite complex, and the evolution of carbonatite magma: REE and isotopic evidence from the Fen complex, southeast Norway. *Chem. Geol. (Isotope Geosciences.)* 65, 147–166.
- Anenburg, M., Mavrogenes, J.A., Frigo, C., Wall, F., 2020. Rare earth element mobility in and around carbonatites controlled by sodium, potassium, and silica. *Sci. Adv.* 6.
- Anenburg, M., Broom-Fendley, S., Chen, W., 2021. Formation of rare earth deposits in carbonatites. *Elements* 17, 327–332.
- Atekwana, E.A., 1996. Precambrian basement beneath the central Midcontinent United States as interpreted from potential field imagery, in van der Pluijm, B.A., Catacosinos, P.A. eds, *Basement and basins of eastern North America*, Geological Society of America Special Paper 308, p. 33–44.
- Banks, D., Yardley, B., Campbell, A., Jarvis, K., 1994. REE composition of an aqueous magmatic fluid: a fluid inclusion study from the Capitan Pluton, New Mexico, USA. *Chem. Geol.* 113, 259–272.
- Blessington, M.J., 2014. A niobium deposit hosted by a magnetite-dolomite carbonatite, Elk Creek Carbonatite Complex, Nebraska, USA: Master's Thesis. University of Nebraska, Lincoln, p. 78.
- Brand, W.A., Coplen, T.B., Vogl, J., Rosner, M., Prohaska, T., 2014. Assessment of international reference materials for isotope-ratio analysis (IUPAC Technical Report). *Pure Appl. Chem.* 86, 425–467. <https://doi.org/10.1515/pac-2013-1023>.
- Brookins, D.G., Treves, S.B., Bolivar, S.L., 1975. Elk Creek, Nebraska carbonatite: strontium geochemistry. *Earth Planet. Sci. Lett.* 28, 79–82.
- Broom-Fendley, S., Styles, M.T., Appleton, J.D., Gunn, G., Wall, F., 2016a. Evidence for dissolution-precipitation of apatite and preferential LREE mobility in carbonatite-derived late-stage hydrothermal processes. *Am. Mineral.* 101, 596–611.
- Broom-Fendley, S., Heaton, T., Wall, F., Gunn, G., 2016b. Tracing the fluid source of heavy REE mineralisation in carbonatites using a novel method of oxygen-isotope analysis in apatite: the example of Songwe Hill, Malawi. *Chem. Geol.* 440, 275–287.
- Broom-Fendley, S., Brady, A.E., Wall, F., Gunn, G., Dawes, W., 2017a. REE minerals at the Songwe Hill carbonatite, Malawi: HREE-enrichment in late-stage apatite. *Ore Geol. Rev.* 81, 23–41.
- Broom-Fendley, S., Wall, F., Spiro, B., Clemens, V., Ullmann, C.U., 2017b. Deducing the source and composition of rare earth mineralizing fluids in carbonatites: insights from isotopic (C, O,  $^{87}\text{Sr}/^{86}\text{Sr}$ ) data from Kangankunde, Malawi. *Contrib. Mineral. Petrol.* 172, 10–23.
- Brown, A., Dougherty, C., Winters, D., Larochele, E., Menard, G., Kuntz, G., St. Onge, J., Tinucci, J., Sames, J., Willow, M.A., Romaniuk, O., Harton, S., 2019. NI 43-101 technical report feasibility study, Elk Creek superalloy materials project, Nebraska, prepared for NioCorp Developments Ltd. [Filing Date May 29, 2019]: Nordmin Engineering Ltd., 596 p., accessed October 10, 2019, at <http://www.sedar.com>.
- Bühn, B., 2008. The role of the volatile phase for REE and Y fractionation in low-silica carbonate magmas: implications from natural carbonatites, Namibia. *Mineral. Petrol.* 92, 453–470.

- Bühn, B., Rankin, A.H., 1999. Composition of natural, volatile-rich Na-Ca-REE-Sr carbonatitic fluids trapped in fluid inclusions. *Geochim. Cosmochim. Acta* 63, 3781–3797.
- Bühn, B., Rankin, A.H., Schneider, J., Dulski, P., 2002. The nature of orthomagmatic, carbonatitic fluids precipitating REE, Sr-rich fluorite: fluid-inclusion evidence from the Okorusu fluorite deposit, Namibia. *Chem. Geol.* 186, 75–98.
- Burfeind, W.J., Carlson, M.P., Smith, R., 1971. The Elk Creek geophysical anomaly, Johnson and Pawnee Counties, Nebraska. *Geol. Soc. Am. Abs. Prog.* 3 (4), 254.
- Carlson, M.P., Treves, S.B., 2005. The Elk Creek carbonatite, Southeast Nebraska—an overview. *Nat. Resour. Res.* 14, 39–45.
- Chacko, T., Mayeda, T.K., Clayton, R.N., Goldsmith, J.R., 1991. Oxygen and carbon isotope fractionations between CO<sub>2</sub> and calcite. *Geochim. Cosmochim. Acta* 55, 2867–2882.
- Chakhmouradian, A.R., Reguir, E.P., Couëslan, C., Yang, P., 2016. Calcite and dolomite in intrusive carbonatites. II. Trace-element variations. *Mineral. Petrol.* 110, 361–377.
- Chakhmouradian, A.R., Reguir, E.P., Zaitsev, A.N., Couëslan, C., Xu, C., Kynicky, J., Mumin, A.H., Yang, P., 2017. Apatite in carbonatitic rocks: Compositional variation, zoning, element partitioning and petrogenetic significance. *Lithos* 275, 188–213.
- Chakhmouradian, A.R., Wall, F., 2012. Rare earth elements: minerals, mines, magnets (and more). *Elements* 8, 333–340.
- Cui, H., Zhong, R., Xie, Y.L., Yuan, X., Liu, X., Brugger, J., Yu, C., 2020. Forming sulfate- and REE-rich fluids in the presence of quartz. *Geology* 48, 145–148.
- Dahlgren, S., 2019. REE mineralization in the Fen Carbonatite Complex, Telemark, Norway - A world-class exploration target for the Hi-Tech and “Green-shift” Industry? Report for the Geological Advisor, 1-2019, 86 p.
- Deines, 1989. Stable isotope variations in carbonatites. In *Carbonatites: Genesis and Evolution* (ed. K. Bell). Unwin Hyman, London, 105–148.
- Demény, A., Sitnikova, M., Karchevsky, P., 2004. Stable C and O isotope compositions of carbonatite complexes of the Kola Alkaline Province: phosphorite–carbonatite relationships and source compositions. In: Wall, F., Zaitsev, A.N. (Eds.), *Phosphorites and Carbonatites from Mantle to Mine: The Key Example of the Kola Alkaline Province*. The Mineralogical Society, London, pp. 407–431.
- DePaolo, D.J., 1981. Neodymium isotopes in the Colorado Front Range and crust – mantle evolution in the Proterozoic. *Nature* 291, 193–197.
- Dietzel, C.A.F., Kristandt, T., Dahlgren, S., Giebel, R.J., Marks, M.A.W., Wenzel, T., Markl, G., 2019. Hydrothermal processes in the Fen alkaline-carbonatite complex, southern Norway. *Ore Geol. Rev.* 111, 1–18.
- Downes, P.J., Demény, A., Czuppon, G., Jaques, A.L., Verrall, M., Sweetapple, M., Adams, D., McNaughton, N.J., Gwalani, L.G., Griffin, B.J., 2014. Stable H-C-O isotope and trace element geochemistry of the Cummins Range Carbonatite Complex, Kimberley region, Western Australia: implications for hydrothermal REE mineralization, carbonatite evolution and mantle source regions. *Miner. Deposita* 49, 905–932.
- Drenth, B.J., 2014. Geophysical expression of a buried niobium and rare earth element deposit: The Elk Creek carbonatite, Nebraska, USA: Interpretation 2, SJ169-SJ179.
- Elliott, H.A.L., Wall, F., Chakhmouradian, A.R., Siegfried, P.R., Dahlgren, S., Weatherley, S., Finch, A.A., Marks, M.A.W., Dowman, E., Deady, E., 2018. Fenites associated with carbonatite complexes: a review. *Ore Geol. Rev.* 93, 38–59.
- Fan, H.R., Yang, K.F., Hu, F.F., Liu, S., Wang, K.Y., 2016. The giant Bayan Obo REE-Nb-F deposit, China: Controversy and ore genesis. *Geosci. Front.* 7, 335–344.
- Farmer, G.L., Broxton, D.E., Warren, R.G., Pickthorn, W., 1991. Nd, Sr, and O isotopic variations in metaluminous ash-flow tuffs and related volcanic rocks at the Timber Mountain/Oasis Valley Caldera Complex, SW Nevada: implications for the origin and evolution of large-volume silicic magma bodies. *Contrib. Miner. Petrol.* 109, 53–68.
- Feng, M., Song, W., Kynicky, J., Smith, M., Cox, C., Kotlanovad, M., Brtnicky, M., Fua, W., Wei, V., 2020. Primary rare earth element enrichment in carbonatites: evidence from melt inclusions in Ulgii Khidi carbonatite, Mongolia. *Ore Geol. Rev.* 117, 103294.
- Gittins, J., 1989. The origin and evolution of carbonatite magmas. In *Carbonatites: Genesis and Evolution*, Bell, K. (ed.) London, 580–600.
- Gysi, A.P., Williams-Jones, A.E., 2013. Hydrothermal mobilization of pegmatite-hosted REE and Zr at Strange Lake, Canada: a reaction path model. *Geochim. Cosmochim. Acta* 122, 324–352.
- Gysi, A.P., Williams-Jones, A.E., 2015. The thermodynamic properties of bastnäsite-(Ce) and parisite-(Ce). *Chem. Geol.* 392, 87–101.
- Gysi, A.P., Williams-Jones, A.E., Harlov, D., 2015. The solubility of xenotime-(Y) and other HREE phosphates (DyPO<sub>4</sub>, ErPO<sub>4</sub> and YbPO<sub>4</sub>) in aqueous solutions from 100 to 250°C and psat. *Chem. Geol.* 401, 83–95.
- Harlov, D.E., 2015. Apatite: A fingerprint for metasomatic processes. *Elements* 11, 171–176.
- Harlov, D.E., Forster, H.J., Njland, T.G., 2002. Fluid-induced nucleation of (Y + REE) -phosphate minerals within apatite: Nature and experiment. Part I. Chlorapatite. *Am. Mineral.* 87, 245–261.
- Harlov, D.E., Wirth, R., Forster, H.J., 2005. An experimental study of dissolution-precipitation in fluorapatite: Fluid infiltration and the formation of monazite. *Contrib. Miner. Petrol.* 150, 268–286.
- Horita, J., 2014. Oxygen and carbon isotope fractionation in the system dolomite–water–CO<sub>2</sub> to elevated temperatures. *Geochim. Cosmochim. Acta* 129, 111–124.
- Hornig-Kjarsgaard, I., 1998. Rare earth elements in sövitic carbonatites and their mineral phases. *J. Petrol.* 39, 2105–2121.
- Ionov, D., Harmer, R.E., 2002. Trace element distribution in calcite-dolomite carbonatites from Spitskop: inferences for differentiation of carbonatite magmas and the origin of carbonates in mantle xenoliths. *Earth Planet Science Letters* 198, 495–510.
- Jago, B.C., Gittins, J., 1991. The role of fluorine in carbonatite magma evolution. *Nature* 349 (6304), 56–58.
- Jebrack, M., 1997. Hydrothermal breccias in vein-type ore deposits: a review of mechanisms, morphology and size distribution. *Ore Geol. Rev.* 12, 111–134.
- Joeckel, R.M., Nicklen, B.L., 2007. Late Paleozoic Weathering and Residual Accumulation of Mineral on Elk Creek Carbonatite, Southeastern Nebraska. Geological Society of America Annual Meeting, Denver, USA.
- Jones, A.P., Genge, M., Carmody, L., 2013. Carbonate melts and carbonatites. *Rev. Mineral. Geochem.* 75, 289–322.
- Karl, N.A., Knudsen, L.D., Mauk, J.L., 2021. Niobium deposits in the United States: U.S. Geological Survey data release, <https://doi.org/10.5066/P914NFSN>.
- Keppler, H., 2003. Water solubility in carbonatite melts. *Am. Mineral.* 88, 1822–1824.
- Kim, S.-T., Coplen, T.B., Horita, J., 2015. Normalization of stable isotope data for carbonate minerals: Implementation of IUPAC guidelines. *Geochim. Cosmochim. Acta* 158, 276–289. <https://doi.org/10.1016/j.gca.2015.02.011>.
- Koenig, A.E., Rogers, R.R., Trueman, C.N., 2009. Visualizing fossilization using laser ablation-inductively coupled plasma-mass spectrometry maps of trace elements in Late Cretaceous bones. *Geology* 37, 511–514.
- Le Bas, M.J., 1999. Sövite and alkavite: two chemically distinct calcio-carbonatites C1 and C2. *S. Afr. J. Geol.* 102, 109–121.
- Le Maître, R.W. (Ed.), 2002. *Igneous Rocks: a Classification and Glossary of Terms*. Cambridge University Press, Cambridge, U.K. p. 193.
- Liu, Y., Chen, Z.Y., Yang, Z.S., Sun, X., Zhu, Z.M., Zhang, Q.C., 2015. Mineralogical and geochemical studies of brecciated ores in the Dalucao REE deposit, Sichuan Province, southwestern China. *Ore Geol. Rev.* 70, 613–636.
- Louvel, M., Bordage, A., Testemale, D., Zhou, L., Mavrogenes, J., 2015. Hydrothermal controls on the genesis of REE deposits: insights from an in situ XAS study of Yb solubility and speciation in high temperature fluids (T<400 °C). *Chem. Geol.* 417, 228–237.
- Louvel, M., Etschmann, B., Guan, Q., Testemale, D., Brugger, J., 2022. Carbonate complexation enhances hydrothermal transport of rare earth elements in alkaline fluids. *Nat. Commun.* 13.
- Mariano, A., 1976. Descriptive Petrography of Selective Drill Core From EC-4. Molycorp Internal Report, Elk Creek, Nebraska.
- Mariano, A.N., 1989a. Nature of economic mineralization in carbonatites and related rocks. In: Bell, K. (Ed.), *Carbonatites: genesis and evolution*, 149–176.
- Mariano, A.N., 1989b. Economic geology of rare earth elements. In: Lipin, B.R. and McKay, G.A. (Eds.), *Geochemistry and Mineralogy of Rare Earth Elements, Reviews in Mineralogy* 21, 309–337.
- Migdisov, A.A., Reukov, V.V., Williams-Jones, A.E., 2006. A spectrophotometric study of neodymium(III) complexation in sulfate solutions at elevated temperatures. *Geochim. Cosmochim. Acta* 70, 983–992.
- Migdisov, A.A., Williams-Jones, A.E., Wagner, T., 2009. An experimental study of the solubility and speciation of the Rare Earth Elements (III) in fluoride- and chloride-bearing aqueous solutions at temperatures up to 300 C. *Geochim. Cosmochim. Acta* 73, 7087–7109.
- Migdisov, A.A., Williams-Jones, A.E., 2014. Hydrothermal transport and deposition of the rare earth elements by fluorine-bearing aqueous liquids. *Miner. Deposita* 49, 987–997.
- Migdisov, A.A., Williams-Jones, A.E., Brugger, J., Caporuscio, F.A., 2016. Hydrothermal transport, deposition, and fractionation of the REE: experimental data and thermodynamic calculations. *Chem. Geol.* 439, 13–42.
- Mitchell, R.H., 2005. Carbonatites and carbonates and carbonates. *Canad. Mineral.* 43, 2049–2068. <https://doi.org/10.2113/gscanmin.43.6.2049>.
- Nadeau, O., Stevenson, R., Jébrak, M., 2018. Interaction of mantle magmas and fluids with crustal fluids at the 1894 Ma Montviel alkaline-carbonatite complex, Canada: insights from metasomatic and hydrothermal carbonates. *Lithos* 296. <https://doi.org/10.1016/j.lithos.2017.11.027>.
- Nicklen, B.L., Joeckel, R.M., 2001. Preliminary report on some prelate Pennsylvanian supra-basement weathering profiles in Southeastern Nebraska. GSA Annual Meeting.
- Panina, L.I., Motorina, I.V., 2008. Liquid immiscibility in deep-seated magmas and the generation of carbonatite melts. *Geochem. Int.* 46, 448–464.
- Perry, E.P., Gysi, A.P., 2018. Rare earth elements in mineral deposits: speciation in hydrothermal fluids and partitioning in calcite. *Geofluids* 1–19.
- Pineau F., Javoy M., and Allégre C. J., 1973. Étude systématique des isotopes de l’oxygène, du carbone et du strontium dans les carbonatites. *Geochim. Cosmochim. Acta* 37, 2363–2377.
- Poitrasson, F., Oelkers, E., Schott, J., Montel, J.-M., 2004. Experimental determination of synthetic NdPO<sub>4</sub> monazite endmember solubility in water from 21°C to 300°C: implications for rare earth element mobility in crustal fluids. *Geochim. Cosmochim. Acta* 68, 2207–2221.
- Premo, W. R., Lowers, H. A., 2013. Age and Origin of Pyroxenites from the Iron Hill Carbonatite Complex, Gunnison, Colorado: Evidence from Pb-Sr-Nd Isotopes: Rocky Mountain Section of the Geological Society of America and Associated Societies Abstracts with Programs 45, p. 12.
- Prokopyev, I.R., Borisenko, A.S., Borovikov, A.A., Pavlova, G.G., 2016. Origin of REE-rich ferrocarnatites in southern Siberia (Russia): implications based on melt and fluid inclusions. *Mineralol. Petrol.* 110, 845–859.
- Ranta, E., Stockmann, G., Wagner, T., Fusswinkel, T., Sturkell, E., Tollefsen, E., Skelton, A., 2018. Fluid-rock reactions in the 1.3 Ga siderite carbonatite of the Gronnedal-Ika alkaline complex, Southwest Greenland. *Contrib. Miner. Petrol.* 173, 1–26.
- Ray, J.S., Ramesh, R., 2000. Rayleigh fractionation of stable isotopes from a multicomponent source. *Geochim. Cosmochim. Acta* 64, 299–306.

- Richet, P., Bottinga, Y., Janoy, M., 1977. A review of hydrogen, carbon, nitrogen, oxygen, sulphur, and chlorine stable isotope enrichment among gaseous molecules. *Annual Rev. Earth Planet. Sci.* 5, 65–110.
- Santos, R.V., Clayton, R.N., 1995. Variation of oxygen and carbon isotopes in carbonatites: a study of Brazilian alkaline complexes. *Geochim. Cosmochim. Acta* 59, 1339–1352.
- Sillitoe, R.H., 1985. Ore-related Breccias in volcanoplutonic arcs. *Econ. Geol.* 80, 1467–1514.
- Smith, M.P., Henderson, P., 2000. Preliminary fluid inclusion constraints on fluid evolution in the Bayan Obo Fe-REE-Nb deposit, Inner Mongolia, China. *Econ. Geol.* 95, 1371–1388.
- Smith, M.P., Henderson, P., Campbell, L.S., 2000. Fractionation of the REE during hydrothermal processes: constraints from the Bayan Obo Fe-REE-Nb deposit, Inner Mongolia, China. *Geochim. Cosmochim. Acta* 64, 3141–3160.
- Smith, M.P., Kynicky, J., Xu, C., Song, W., Spratt, J., Jeffries, T., Brtnicky, M., Kopriva, A., Cangelosi, D., 2018. The origin of secondary heavy rare earth element enrichment in carbonatites: constraints from the evolution of the Huanglongpu district, China. *Lithos* 308–309, 65–82.
- Song, W., Xu, C., Smith, M.P., 2018. Genesis of the world's largest rare earth element deposit, Bayan Obo, China: protracted mineralization evolution over 1 b.y. *Geology* 46, 323–326.
- Taylor, H.P., Frechen, J., Degens, E.T., 1967. Oxygen and carbon isotope studies of carbonatites from the Laacher See district, West Germany and the Alnö district, Sweden. *Geochim. Cosmochim. Acta* 31, 407–430.
- Trofanenko, J., Williams-Jones, A.E., Simandl, G.J., Migdisov, A.A., 2016. The nature and origin of the REE mineralization in the Wicheeda Carbonatite, British Columbia, Canada. *Econ. Geol.* 111, 199–223.
- Van Schmus, W.R., Bickford, M.E., Turek, A., 1996. Proterozoic geology of the east-central Midcontinent basement. In: van der Pluijm, B.A., Catacosinos, P.A. (Eds.), *Basement and Basins of Eastern North America*. Geological Society of America Special Paper, Boulder, Colorado, pp. 7–32.
- Verplanck, P.L., Van Gosen, B.S., Seal, R.R.II, McCafferty, A.E., 2014. A deposit model for carbonatite and peralkaline intrusion-related rare earth element deposits: U.S. Geological Survey Scientific Investigations Report 2010-5070-J, 58 p.
- Verplanck, P.L., Mariano, A.N., Mariano, A.N. Jr, 2016. Rare earth element ore geology of carbonatites, in Verplanck, P.L., and Hitzman, M.W., eds, *Society of Economic Geologists Reviews in Economic Geology* 18, 5–32.
- Verplanck, P.L., Lowers, H.A., Johnson, C.A., Koenig, A. E., Kettler, R.M., and Joeckel, R. M., 2022. Geochemical data for the Elk Creek alkaline complex, southeast Nebraska. U.S. Geological Survey data release. <https://doi.org/10.5066/P9S41SV0>.
- Wall, F., Mariano, A.N., 1996. Rare earth minerals in carbonatites: a discussion centered on the Kangankunde Carbonatite, Malawi. In: Jones, A.P., Wall, F., Williams, C.T. (Eds.), *Rare Earth Minerals: Chemistry Origin and Ore Deposits*. Chapman and Hall, London, pp. 193–226.
- Walter, B.F., Giebel, R.J., Steele-MacInnis, M., Marks, M.A.W., Kolb, J., Markl, G., 2021. Fluids associated with carbonatitic magmatism: a critical review and implications for carbonatite magma ascent. *Earth Sci. Rev.* 215 <https://doi.org/10.1016/j.earscirev.2021.103509>.
- Wang, Z.-Y., Fan, H.-R., Lingli, Z., Yang, K.-F., She, H.-D., 2020. Carbonatite-related REE deposits: an overview. *Minerals* 10, 965.
- Whitmeyer, S.J., Karlstrom, K.E., 2007. Tectonic model for the Proterozoic growth of North America. *Geosphere* 3, 220–259.
- Williams-Jones, A.E., Samson, I.M., Olivo, G.R., 2000. The genesis of hydrothermal fluorite-REE deposits in the Gallinas Mountains, New Mexico. *Econ. Geol.* 95, 327–341.
- Williams-Jones, A.E., Migdisov, A.A., Samson, I.M., 2012. Hydrothermal mobilization of the rare earth elements—a tale of “ceria” and “yttria”. *Elements* 8, 355–360.
- Woolley, A.R., 1982. A discussion of carbonatite evolution and nomenclature and the generation of sodic and potassic fenites. *Mineral. Mag.* 46, 13–17.
- Woolley, A.R., Kempe, D.R.C., 1989. Carbonatites: Nomenclature, average chemical compositions and element distribution. In: Bell, K. (Ed.), *Carbonatites: Genesis and Evolution*. Unwin Hyman, London, pp. 1–14.
- Xie, Y.L., Hou, Z., Yin, S., Dominy, S.C., Xu, J., Tian, S., Xu, W., 2009. Continuous carbonatitic melt–fluid evolution of a REE mineralization system: Evidence from inclusions in the Maoniuping REE Deposit, Western Sichuan, China. *Ore Geol. Rev.* 36, 90–105.
- Xie, Y.L., Li, Y.X., Hou, Z.Q., Cooke, D.R., Danyushevsky, L., Dominy, S.C., Yin, S.P., 2015. A model for carbonatite hosted REE mineralisation - the Mianning-Dechang REE belt, Western Sichuan Province, China. *Ore Geol. Rev.* 70, 595–612.
- Ying, Y.-A., Chen, W., Simonetti, A., Jiang, S.-Y., Zhao, K.-D., 2020. Significance of hydrothermal reworking for REE mineralization associated with carbonatite: Constraints from in situ trace element and C-Sr isotope study of calcite and apatite from the Miaoya carbonatite complex (China). *Geochim. Cosmochim. Acta* 280, 340–359.
- Zaitsev, A.N., Demény, A., Sindern, S., Wall, F., 2002. Burbankite group minerals and their alteration in rare earth carbonatites. source of elements and fluids (evidence from C-O and Sr-Nd isotopic data). *Lithos* 62, 15–33.